DISSERTATION

RELATIVE RESPONSE OF ALANINE AND FILTERED ALANINE ELECTRON PARAMAGNETIC RESONANCE DOSIMETRY IN MIXED NEUTRON-GAMMA FIELDS

Submitted by

Paige K. Witter

Department of Environmental and Radiological Health Sciences

In partial fulfillment of the requirements

For the Degree of Doctor of Philosophy

Colorado State University

Fort Collins, Colorado

Summer 2025

Doctoral Committee:

Advisor: Alexander Brandl

Thomas E. Johnson
William Brazile
Adam Chicco

ABSTRACT

RELATIVE RESPONSE OF ALANINE AND FILTERED ALANINE ELECTRON PARAMAGNETIC RESONANCE DOSIMETRY IN MIXED NEUTRON-GAMMA FIELDS

An electron paramagnetic resonance (EPR) spectroscopy procedure was investigated for use in novel mixed neutron and gamma radiation fields. L-α-alanine ("alanine") is an amino acid that develops stable unpaired electrons when exposed to ionizing radiation. The number of unpaired electrons, measured via EPR, is proportional to the absorbed dose in tissue from photons. The EPR signal dependence on neutrons across different spectra, especially in specific moderated experimental conditions, is less well characterized than for gamma dosimetry. Alanine was exposed to gamma and neutron sources, a variety of neutron spectra, and escalating doses to develop calibration curves for sources at Colorado State University and determine the specific neutron source sensitivity. Neutron exposures have lower cumulative signals than gamma exposures for the same dose and alanine mass, with sensitivities ranging from 0.056 $\pm$0.085 for the Bare PuBe source to 0.245 ± 0.212 for the bare ^{252}Cf. These values are on the low end of literature ranges or below literature sensitivity values for other neutron sources, leading to a hypothesis of a low dose-rate effect in alanine that should be investigated further. Thermal-neutron sensitive filters of cadmium and gadolinium metal foils were added to alanine dosimeters to investigate the signal response. A comparison of the bare- versus filtered signal response in the known mixed fields showed that the filters did not consistently increase the thermal-neutron sensitivity of alanine. At low total doses, where the gamma contribution to the

total dose was very low, the cadmium and gadolinium foils increased the alanine response to the field. When the gamma dose contribution rose to a source-specific point, photon interactions in the foils decreased the photon fluence in the alanine pellets, leading to a decreased dosimeter response. This dual-effect of the thermal-neutron sensitive foils is a novel finding, and should be investigated with source specific gamma spectra. While a filtered-alanine dosimeter is not usable at the current stage, bare alanine calibration curves for the neutron sources at CSU were created and available for subsequent irradiations in various fields at unknown doses.

ACKNOWLEDGEMENTS

To Alex Brandl, thank you for your support, guidance and encouragement, not only with this project but with the health physics field in general. Your open and stated goals about our responsibilities to workers and the public are inspiring at this time, and I'm grateful to be taking that message with me. To my family, and especially my mom, thank you for encouraging me to do things that are difficult: "Why would something being hard mean you wouldn't try it?". It's been a privilege to be close to family over the last six years, and I'm taking that support everywhere I go. Finally, thank you to my partner and soon-to-be husband, who has led a split life with me while we're both in graduate school in different cities. The stresses and struggles are always a little better when you're around.

Thank you also to the CSU Analytical Resources Core for use of the Electron Paramagnetic Resonance Spectrometer, training, and support (RRID: SCR_021758).

TABLE OF CONTENTS

Introduction

Motivation

Neutron dosimetry is a growing field of radiation safety research, due to the existing and new applications where neutron radiation is present. From the discovery of the neutron in 1932, the methods of interaction and the effect on the human body have been constant questions as we harness neutrons for various means. From their presence in nuclear reactors and weapons, in simulating the effects of space radiation, and medical therapies and high-energy particle physics research here at Colorado State University, there are a wide variety of locations where an inexpensive, accurate, and robust neutron dosimeter is needed.

Neutrons present a unique dosimetry challenge: they are uncharged particles and thus have no electromagnetic interactions with surrounding matter. They interact primarily via elastic scattering off atomic nuclei. A single neutron source may be monoenergetic (e.g., a neutron generator), have neutrons across a potentially wide energy spectrum (e.g., a neutron generator in a room with moderators), or even have both neutrons and gammas emitted (e.g., a ^{252}Cf or plutonium-beryllium source, or a criticality event). The dose imparted by neutrons can vary significantly depending on the incident neutron energy and interacting material. Thus, a dosimeter must be able to either a) be calibrated and used in a known dose field or b) be able to take into account an unknown, potentially wide neutron spectrum and potential mixed field to be able to determine the dose. To be used in a variety of neutron energy fields, they must have sensitivity to a wide range of neutron energies, from thermal (0.025 eV) to fast (orders of MeV). They must have an analysis method that is affordable and can be performed within a useful

timeframe. Additionally, they must be of a size that can be easily transported or placed in the locations of interest, whether that is on a body or in an experimental location. This last requirement precludes the majority of neutron spectrometry instruments, which rely on increasingly large amounts of heavy moderating material to slow down neutrons to thermal speeds for detection.

Current wearable neutron dosimeters include CR-39 track-etch dosimeters, personal electronic dosimeters, thermoluminescent dosimeters (TLDs), optically stimulated luminescent dosimeters (OSLs), direct-ion storage dosimeters, and activation foil-based spectrometers (Gómez-Ros, Bedogni, and Domingo 2023). With the exception of activation foil-based spectrometers, the dosimeters do not provide information about the neutron energy spectrum and so their response in the radiation field must be known or calibrated. Activation foil-based dosimeters are comprised of materials with known activation probabilities to specific neutron energies so that activation activity measurements of the foils can be used to deduce the neutron energy spectrum to which the dosimeter is exposed. Determination of the neutron spectrum provides further detail about the radiation field and potential hazard to which a worker is exposed. However, activation-based dosimetry is both time- and labor intensive, often requiring multiple foils to be analyzed, and the analysis window is limited by the half-life of the activation products. For this reason, activation-foil based dosimeters are only used in circumstances where a possible dose would be noted, and the analysis of the dosimeter would occur immediately following an exposure to neutrons (e.g., criticality accident dosimeters or neutron source characterization exercises).

Neutrons are uncharged subatomic particles. Like other uncharged ionizing radiation (e.g., gammas), they can travel substantial distances. The probability that a given type of interaction will occur, known as the *cross section* of interactions, depends both on the incident neutron energy and the identity of the target nuclide. Neutrons are classified according to their energy in broad bands (Table 1), although there is no specific agreement to the classification (NRC 2011). Thermal neutrons are neutrons that are in thermal equilibrium with their environment, and thus their speed distribution follows a Maxwell-Boltzmann distribution. Standard temperature and pressure for thermal neutrons is 20°C (293 K), at 1 atm. The most probable energy in this distribution is 0.025 eV (2200 m/s).

Table 1. Neutron energy classifications.

Classification	Energy range (approximate)
Thermal	0.025 eV
Slow	<10 eV
Intermediate	10 eV- 100 keV
Fast	> 100 keV

The most likely neutron interaction for almost all nuclides and neutron energies is elastic scattering. When the target nucleus has close to the same mass as the incident neutron, the greatest amount of energy can be transferred. Thus, the lower the atomic mass of the target, the more effective it is as a moderator and the more energy is transferred on average from the neutron. Moderators with components with low atomic masses such as hydrogen slow neutrons via elastic scattering. Common moderators include water, paraffin, plastic, and graphite (NRC

2011). Lower energy neutrons have a higher likelihood of interacting with hydrogen than higher energy neutrons (Fig. 1).

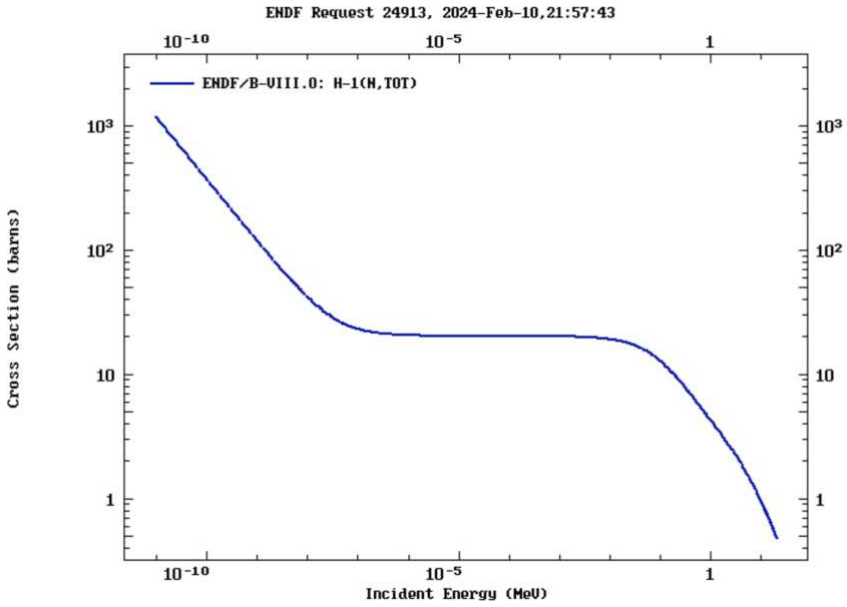

Figure 1**.** ENDF/ B-VIII.0 ^{1}H Total neutron interaction cross section, by neutron energy (Brown et al. 2018).

Neutrons can also interact through charged-particle reactions and capture reactions. In charged particle reactions, a target nucleus absorbs a neutron to form a compound nucleus, which later emits a charged particle (e.g., proton, alpha). Photons may also be emitted if the final nucleus is left in an excited state. An example of a charged particle reaction is the $^{10}\mathrm{B}\ (n,\alpha)\ ^{7}\mathrm{Li}$, with a thermal neutron cross section of 3840 b. A capture reaction can occur if the target nucleus absorbs a neutron, and the resulting nucleus is left in an excited state, which deexcites via prompt gamma emission. An example of a capture reaction is the $^{1}\mathrm{H}\ (n,\gamma)\ ^{2}\mathrm{H}$ reaction, with a thermal neutron cross section of 0.33 b and a 2.22 MeV prompt gamma emission 100% of the time. The secondary particles of these types of neutron interactions can impart dose as well as the prompt gammas (NRC 2011).

Radiation-induced damage and the potential biological effects depend both on the radiation dose and on the type of radiation. In general, neutrons produce greater damage than equivalent doses of gammas (Shuryak et al. 2020; Xu et al. 2015; Stricklin et al. 2021). Neutron-induced secondary particles, such as recoil nuclei and charged particle emissions (e.g., protons, alphas) have high linear energy transfer (LET) compared to photon induced secondary particles (electrons) with low LET. In general, neutrons are more effective at damaging cells (Xu et al. 2015). Up to a point, higher LET radiation shows higher biological effectiveness. Using the biological endpoint of cell killing as an example and starting at low LET, the efficiency of killing increases with LET. This is due to the increase in density of excitations and ionization along the particle tracks in critical cell targets (e.g., DNA). The most efficient LET for killing a cell is reached at around 100- 130 keV μm^{-1}, while further increase in LET results in more energy deposition than is needed for killing. Thus, the RBE decreases at very high LET (Turner 2007).

The absorbed dose from fast neutrons is due almost entirely to the energy transferred to the atomic nuclei in tissue by elastic scattering. A fast neutron loses an average of half its energy in a single collision with hydrogen. This results in a recoil proton (charged particle) that can deposit dose in a local area. For the other nuclei in soft tissue, the average energy loss is about half the maximum energy loss, which is transferred to the nucleus and results in a recoil nucleus. Depending on the energy transfer (fast vs slow incident neutron), the recoil nuclei could act as ionizing particles that deposit energy in the local area of the scatter. Iron in blood (^{56}Fe) has a maximum energy transfer Q_{max} of about 0.089 E_n, with an average energy transfer Q_{avg} of 0.0345 E_n. For high energy incident neutrons such as 14 MeV neutrons, that average energy transfer to

the Fe nucleus is about 0.482 MeV. The recoil Fe nucleus could act like a heavy charged particle in the local area of the scatter interaction.

The recoil nuclei deposit dose in the local area and thus are what contribute to the biological effects of the radiation. Thus, neutron RBE may be comparable to heavy charged particle RBE, especially if the energy of the recoil nuclei and the quantity of scatter interactions is similar to the energy of incident heavy charged particles and their flux.

The dose from slow and thermal neutrons comes primarily from capture reactions in ^{1}H and ^{14}N in tissue. The $^{1}H(n, \gamma)^{2}H$ reaction releases a 2.22 MeV gamma ray, which could deposit some of its energy via Compton scattering prior to escaping the body. Thus, this reaction does not contribute much to neutron RBE. However, the $^{14}N(n, p)^{12}C$ capture releases 0.626 MeV, shared by the proton and recoil carbon nucleus, and deposited in the local area of the capture site (Turner 2007). This energy deposition could be similar to heavy charged particle depositions of incident carbon or similarly sized ions and thus contribute to why neutron RBE may be comparable to heavy charged particle RBE.

The radiation weighting factor, w_R, is a dimensionless factor that reflects the relative biological effectiveness of a specific radiation type (and in the case of neutrons, is dependent on energy). It multiplies with the mean absorbed dose in a tissue or organ to obtain the equivalent dose. In contrast to the quality factor of a radiation, the w_R is defined for the radiation incident on a target, not for the particles that deposit dose (since those may be different than the incident radiation type). w_R is used by ICRP for protection quantities. w_R values are based on experimental data for the RBE of radiation at low doses, specifically the magnitude of the low-dose maximum RBE (RBEM) for late stochastic effects, especially cancer, in humans.

The biological effectiveness of neutrons incident on the human body is strongly dependent on neutron energy due to the previously discussed interaction mechanisms of neutrons of varying energies. Low-energy neutrons primarily deposit dose via ^{1}H and ^{14}N capture reactions, while higher energy neutrons deposit dose via recoil nuclei from elastic scattering. The damage and biological effects caused by neutrons varying in energy is reflected in the continuous function of the radiation weighting factor for neutrons (Equation 1 and Fig. 2) (Boice Jr. et al. 2012):

$$w_R = \begin{cases} 2.5 + 18.2e^{-\frac{[ln(E_n)]^2}{6}} \\ 5.0 + 17.0e^{-\frac{[ln(2E_n)]^2}{6}} \\ 2.5 + 3.25e^{-\frac{[ln(0.04E_n)]^2}{6}} \end{cases} \quad \text{Eq. 1}$$

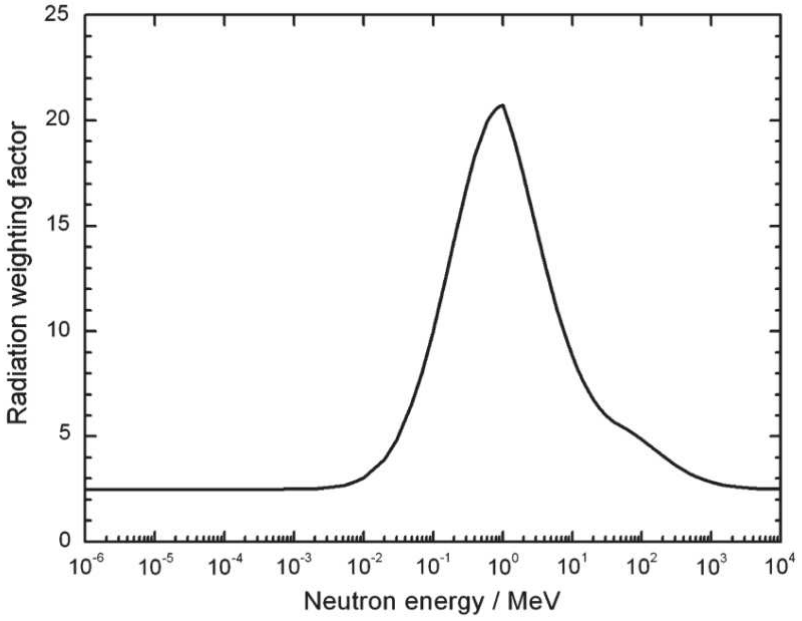

Figure 2**.** Radiation weighting factor, w_R, for neutrons versus neutron energy (Boice Jr. et al. 2012).

Since neutrons are often present in a wide spectrum of energies, fluence-to-dose conversion factors (FCF) that vary as a function of neutron energy are often used to calculate the

dose quantity of interest from a measured or known spectrum. An effective conversion factor can be calculated using the average neutron energy for an energy region where the FCF is relatively constant. For regions where the factors vary with energy, FCFs can be determined by calculating the spectrum weighted-average FCF described by

$$\int_{E_1}^{E_2} \Phi(E)\ \mathrm{FCF}(E)\mathrm{d}E\ = \mathrm{FCF}_{\mathrm{eff}} \int_{E_1}^{E_2} \Phi(E)\mathrm{d}(E) \qquad \text{Eq. 2}$$

Where:

FCF(E) = fluence-to-dose conversion factor as a function of energy,

FCF_{eff} = effective fluence-to-dose conversion factor for neutron energies between E1 and E2.

Equation 2 is evaluated either using the methods described above or by Monte Carlo techniques. The resulting FCFs can be used to calculate a spectrum-specific dose rate for a dose quantity of interest; for example, absorbed dose. This project used the fluence-to- personal absorbed dose conversion factors from ANSI N13.3 Table B1 to calculated absorbed dose rate based on measured neutron spectra (ANSI/HPS 2013) .

Electron Paramagnetic Resonance Spectroscopy

Electron paramagnetic resonance (EPR) spectroscopy is the resonant absorption of electromagnetic energy by transition of the spin of an unpaired electron between different energy levels in a paramagnetic substance and in the presence of a magnetic field. Two energy levels, E_1 and E_2, exist for an unpaired electron in a magnetic field. In thermal equilibrium, the population of electrons in the lower level E_1 is slightly higher than in the upper level E_2. Thus, the

system is able to absorb energy from an external high frequency (HF) field (resonance condition) if a relaxation mechanism exists due to interaction with the surrounding medium:

$$E_2 - E_1 = \Delta E = hv \qquad \text{Eq. 3}$$

An EPR spectrometer utilizes an HF field and a magnetic field. A klystron generates microwaves (the HF field) and is coupled to the measurement cavity by a waveguide system. The measurement cavity holds the sample in the magnetic field. The magnetic field is scanned linearly and is modulated by the stable RF field. The absorbed energy from the sample will change the balance of the microwave system, in the resonance condition. In general, the first derivative of the absorption curve is registered as a function of the magnetic field, yielding the typical EPR spectrum (Regulla and Deffner 1982; Bradshaw et al. 1962; Stuglik 2007).

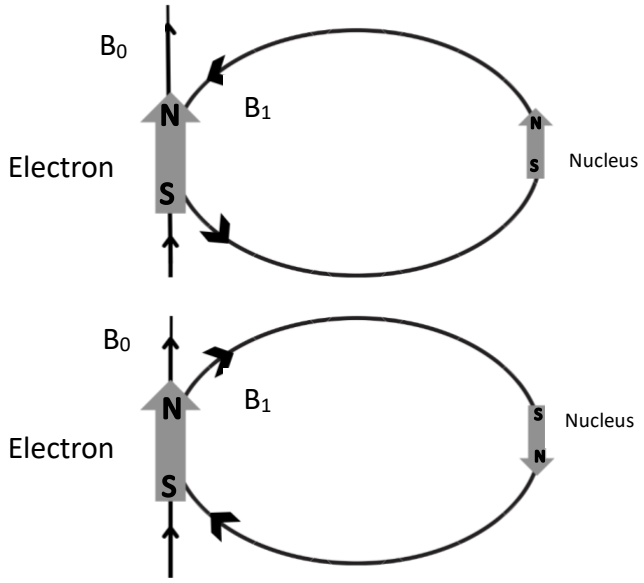

Figure 3**.** Local magnetic field at an electron, B_1, due to a nearby nucleus.

Most organic molecules are diamagnetic, since they usually contain an even number of electrons and thus the net magnetic moment resulting from the electron spins is zero. Since covalent bonds are formed by electrons of opposite spin, the net magnetic moment of pairs of valence electrons in bond formations is also zero. Ionizing radiation can break these bonds, resulting in two paramagnetic parts with an unpaired electron each, called free radicals. The hydrogen atom ^{1}H is the simplest free radical. The rigidity of the matter and the molecular surroundings impact the stability of free radicals. The lifetime of free radicals in solutions or aqueous organic materials is generally very short. However, in some crystalline materials, free radicals may exist for months or even years. The lifetime of a free radical can be impacted by the temperature during the irradiation as well as the structure of the crystal (Regulla and Deffner 1982).

Nuclei of atoms in a molecule often have a magnetic moment producing a local magnetic field at the electron. The interaction between electrons and surrounding nuclei is called a hyperfine interaction, producing a hyperfine EPR spectrum. Hyperfine interaction spectra provide insight into the identity of the radical and the number of atoms and their distances from unpaired electrons. As the number of nuclei gets larger, the number of signals in the EPR spectrum increases exponentially (2^{N}). Amino acids exhibit relatively well-resolved spectra after irradiation. As they can be purified in crystalline form, and often in single crystals, they are convenient for EPR investigation. A free-radical method of dosimetry depends on the lifetime of the radiation-induced radical(s) and the magnitude of radical yield per unit absorbed dose (Regulla and Deffner 1982). Crystalline alanine has both a long-lasting free radical and a relatively large radical yield per unit absorbed dose of gammas, making it a good choice for this type of dosimetry.

Alanine EPR

Alanine is an amino acid that constitutes a high percentage of amino acids in most proteins. It can be produced in crystalline structures and is commercially available in powder or pellet forms. Solid pellets composed of alanine and paraffin, with an alanine content up to 90% by weight, are preferrable for EPR dosimetry. Paraffin positively impacts neutron sensitivity and acts as a binder to allow reasonable reproducibility of pellet dimensions. Paraffin also adds negligible EPR signal when irradiated. The specific gravity of the sample depends on the paraffin content but is close to soft tissue. 50% paraffin has a density of $\rho = 1.05\ \mathrm{g \cdot cm^{-3}}$, while 10% paraffin content has a density of $\rho = 1.22\ \mathrm{g \cdot cm^{-3}}$. L-$\alpha$-alanine was found to be the best material for dosimetry, due to a combination of a low zero-dose reading signal and a high yield of radicals after irradiation. L-alanine from different manufactures have shown no systematic variations in the EPR structure, although the response can vary in neutron fields based on the hydrogen content (Regulla and Deffner 1982; Schraube et al. 1989).

L-α-alanine's radiation-induced paramagnetic resonance was first developed as a gamma radiation dosimeter in 1962, due to its sensitivity to radiation interactions over a wide energy range, the stability of the radiation-induced signal, and its tissue-like properties in absorbing radiation (Bradshaw et al. 1962). Since then, it has become a well-known method for transfer and reference dosimetry. Neutron dosimetry using alanine and alanine doped with thermal-neutron sensitive material has been investigated to increase alanine's response across a wide neutron spectrum (M. Marrale et al. 2007; Maurizio Marrale et al. 2008; M. Marrale et al. 2008; 2015). Alanine has no absorbed dose dependence for doses below 5 kGy (Desrosiers, Puhl, and Cooper 2008). However, dose rate effects have been observed in gamma fields between 1 Gy/s and 2

Gy/s, and lower dose rates have less investigation due to alanine's prevalence as a high-dose dosimeter (Desrosiers, Puhl, and Cooper 2008; Desrosiers and Puhl 2009). Additionally, alanine has been used in multiple criticality accident intercomparison exercises, in which the dose is imparted in a single critical flash (Trompier et al. 2004; F. Trompier et al. 2008). Alanine's inexpensive material costs, as well as the availability of a Bruker Elexsys II E500 EPR spectrometer in the Colorado State University Analytical Resources Core (ARC), make it an ideal method for further research to investigate novel neutron dosimetry methods, especially those that could be used at CSU for future research needs.

L-α-alanine electron paramagnetic resonance (alanine EPR) dosimetry is an existing and growing option that addresses concerns with other dosimeter types, specifically:

i) Wide dose-detection range (0.5 Gy – 100 kGy).

ii) Linear dose-response dependence (up to 10 kGy).

iii) Non-toxic, easy to handle and wear.

iv) Tissue equivalency (similar interaction mechanisms to human tissue).

v) Quick dose readout (< 3 min).

vi) Stability of the dosimetric signal over months to years (Stuglik 2007).

vii) Commercially available and inexpensive dosimetric material.

Downsides of a pure-alanine neutron dosimeter include that alanine is more sensitive to photons than neutrons, more sensitive to fast than thermal neutrons, and has a relatively high minimum detectable dose. Therefore, in a mixed field (neutrons plus photons), a photon dosimeter or knowledge of the neutron-to gamma dose ratio is needed to subtract out the gamma component. Neutron sensitivity, especially to thermal neutrons, has been shown to be increased via the

addition of doping agents to alanine pellets (Bartolotta et al. 1999; M. Marrale et al. 2007; 2015). The development of an alanine-based neutron dosimeter with multiple alanine elements sensitive to different regions of the neutron energy spectrum is ongoing and an area of active research. The use of neutron-sensitive materials surrounding alanine to increase specific energy sensitivities is also starting to be investigated (Romanyukha 2021). Finally, it was possible to reduce the minimum detectable dose using a combination of signal acquisition and signal processing techniques, such as dosimeter rotation during measurement, use of an EPR standard in the resonator, subtraction of background, non-radiogenic signals, and polynomial filtration of the EPR spectrum (Hayes et al. 2000).

The interaction of ionizing radiation with alanine triggers breaks in molecular bonds, giving rise to stable radicals within the crystalline structure. The most stable radical, and the predominate radical formed at room temperature, corresponds to the breaking of the NH_2 group (Fig. 4).

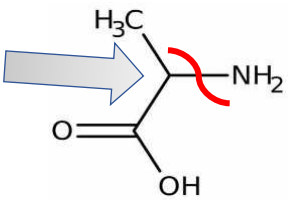

Figure 4. Alanine and the radical formation after radiation-induced damage.

Alanine radicals exhibit a hyperfine structure in the EPR spectrum due to the coupling with the four surrounding hydrogen protons. The central carbon C-H bond is responsible for the central line of the spectrum. At room temperature, the three methyl (CH_3) protons with the radical are

magnetically equivalent and interchange quickly by tunnelling or rotation, producing the other peaks in the spectrum (Regulla and Deffner 1982).

The most common representation of the EPR spectrum is the first derivative of the paramagnetic absorption spectra and is supplied by the routine readout procedure (Fig. 5). Two methods have commonly been used for dose assessment. The double-integrated ESR spectra (the area under the first derivative curve) can be used, with integration performed graphically, with a computer, or electronically. Alternatively, if the ESR spectrum is not dose-dependent (i.e., the hyperfine structure does not change with dose) and there are negligible secondary radical reactions, an amplitude of one or all of the first derivative peaks can be taken as a relative measurement of the concentration of free radicals. Signal noise, base line drift, and background signals can all affect these methods. Alanine shows an identical EPR spectrum for doses ranging from 1 Gy to 10^4 Gy, thus the peak-to-peak amplitude can be used as a representative dosimetric reading. The units used can be arbitrary (e.g., millimeters, “signal”, arbitrary units “a.u”). The EPR spectrometer gain factor must be taken into account for this type of quantitative comparison (Regulla and Deffner 1982). The peak-to-peak amplitude method is the preferred method whenever integrators are not available.

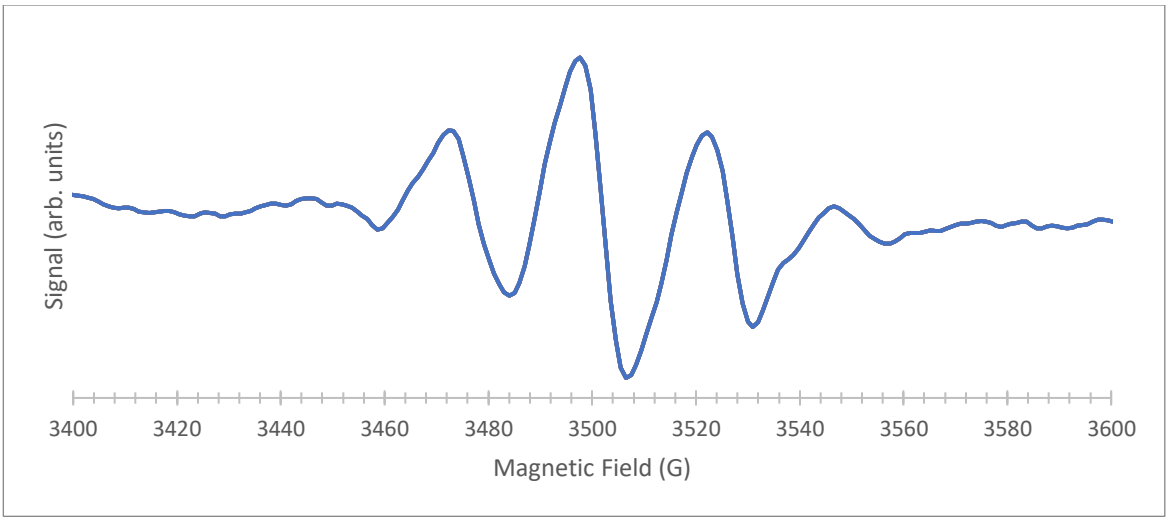

Figure 5. ^{137}Cs Irradiated Alanine EPR spectra with the hyperfine peaks produced by the free radical.

Alanine Sensitivity to Neutron Radiation

Relative sensitivity factors for neutron irradiation are determined in order to compare to a standard gamma irradiation (Trompier et al. 2004; Katsumura et al. 1986; Schraube et al. 1989; Waligorski et al. 1989). A calibration curve from reference dosimetry (e.g., ^{60}Co or ^{137}Cs) is used to estimate the alanine EPR response for a given dose, and the relative neutron sensitivity is calculated as the neutron response divided by the difference of the expected response to a total dose and the response to the expected gamma dose of that exposure. This relative sensitivity factor can then be used to relate the EPR signal from a neutron exposure to a calibration curve made from gamma exposures. Reported neutron sensitivity factors range from 0.20 ± 0.18 in bare reactor spectra, to 0.83 ± 0.09 in a 20 MeV monoenergetic neutron beam. They can also vary by the quantity of paraffin in the alanine pellet (Trompier et al. 2004; Katsumura et al. 1986). Due to the variations in alanine sensitivity to neutrons of different energies, a relative sensitivity factor is dependent on the neutron energy and thus should be calculated for each source separately.

Neutron relative sensitivity factors were calculated for each source and experimental condition (presence of filter) in this study.

Dosimetry Needs at Colorado State University

There are a variety of neutron and mixed neutron/gamma sources at CSU. The characterization of the alanine EPR response to three sources was the focus of this project:

a) A 6000 Ci ceasium-137 (^{137}Cs) gamma source (calibration, installed November 1976),
b) a 41.78 mCi californium-252 (^{252}Cf) mixed neutron/gamma source (installed June 2023),
c) a 5 Ci plutonium-beryllium (Pu-Be) mixed neutron/gamma source.

Additionally, the use of filters to target and increase alanine response to specific parts of the neutron spectrum was investigated and characterized within each field. Specifically, the filters investigated were:

a) Cadmium (^{113}Cd):
    a. σ_{th} =19860 b,
    b. ($n + {}^{113}Cd \rightarrow {}^{114}Cd^{*} \rightarrow \gamma + {}^{114}Cd$),
    c. photon component hypothesized to increase interaction response in alanine (Fig. 6).
b) Gadolinium (Gd)
    a. Two stable isotopes: ^{155}Gd (σ_{th} = 75,000 b, atomic fraction 0.148) and ^{157}Gd (σ_{th} = 250,000 b, atomic fraction 0.156):
    b. $\sigma_{th,eff}$ =50,000 b (Fig. 7),

c. After neutron capture, prompt gamma capture by inner-shell electron leading to Auger emission. Auger electron component hypothesized to increase interaction response in alanine.

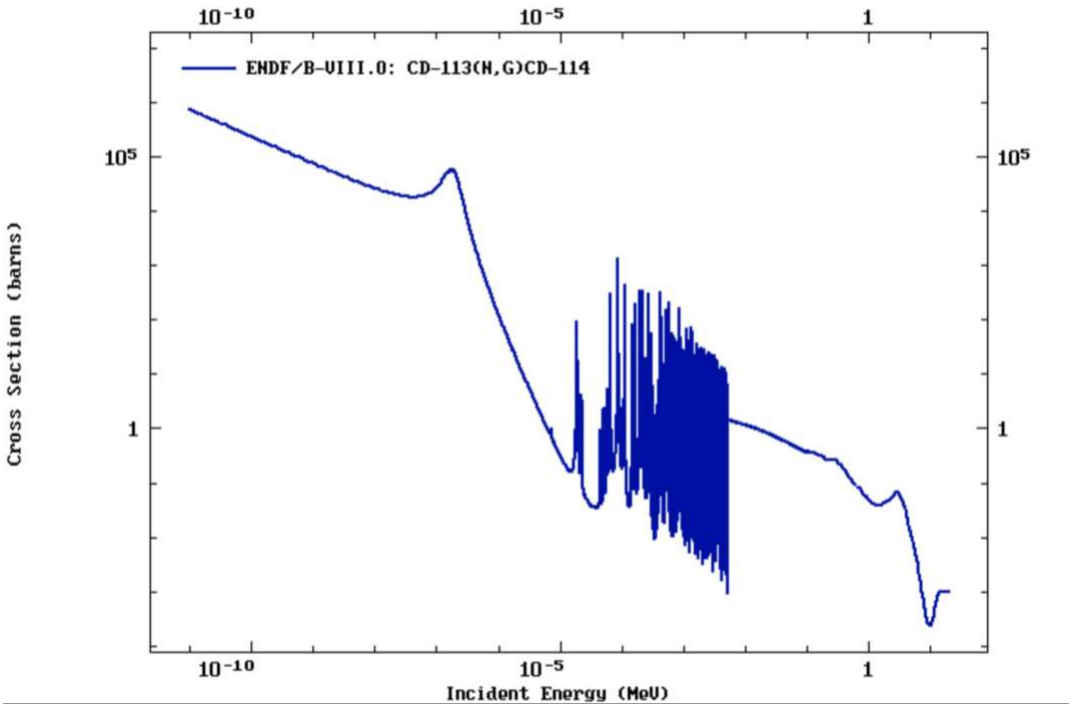

Figure 6. $^{113}\mathrm{Cd}\ (n,\gamma)\ ^{114}\mathrm{Cd}$ neutron absorption cross section (Brown et al. 2018).

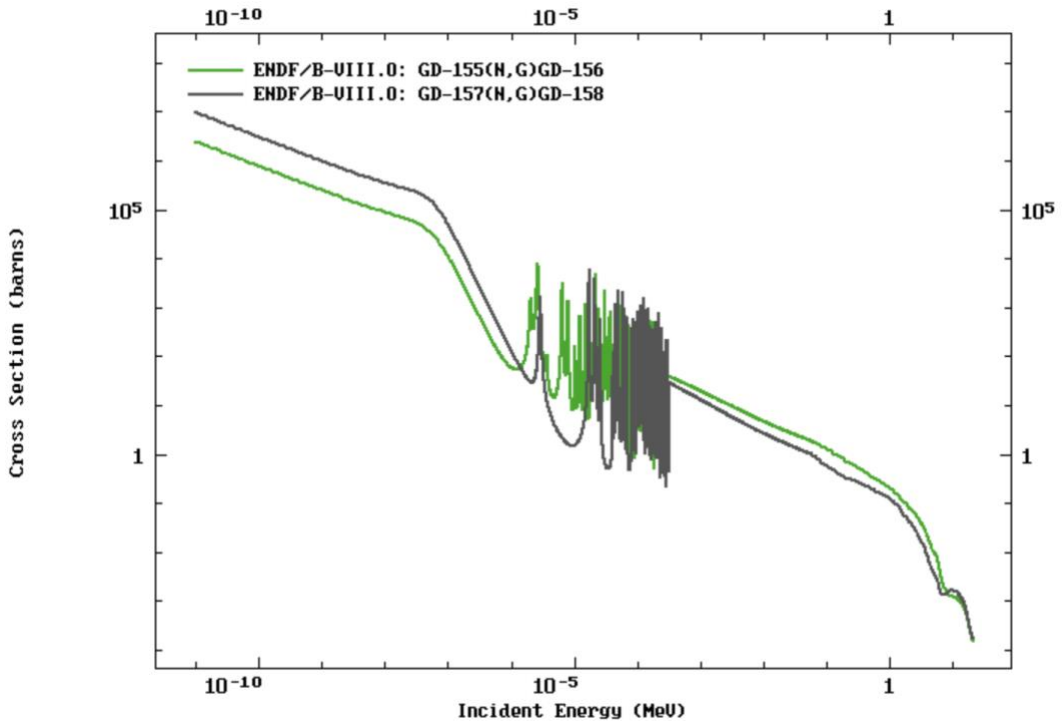

Figure 7. ^{155}Gd and ^{157}Gd (n,γ) neutron absorption cross sections (Brown et al. 2018).

Neutron Spectrometry

In order to produce a dose-response calibration curve for unknown doses, the dose rate and dose field must first be determined. Bonner sphere spectrometry (BSS) and neutron spectrum unfolding were used to characterize the ^{252}Cf source and Pu-Be source.

Bonner spheres are a neutron detector set involving a thermal neutron detector (^{6}Li crystal scintillation) at the center of spherical high-density polyethylene (HDPE) moderators of increasing sizes (2, 3, 5, 8, 10, and 12 inches) (Fig. 8). The response function of the moderator+detector pair is represented as the response and efficiency of the detector set as a function of incident (monoenergetic) neutrons. As the size of the moderator changes, the shape of the response function changes. The peak of the response function shifts to higher neutron

energies as the size of the moderator increases. The integral over the neutron energy spectrum relates the number of counts registered by the detector to the detector's response function:

$$N_i + \epsilon_i = \int R_i\,(E) \cdot f(E)\;\; dE \qquad \text{Eq. 4}$$

where:

N_i = number of counts registered by detector I,

ϵ_i = unknown measurement error of the detector,

$R_i(E)$ = response function of the detector to the neutron energy E, and

$f(E)$ = neutron energy spectrum.

Using a finite number of measurements (i.e., measurements from a set of moderating spheres), there is not a unique solution for deriving $f(E)$, the incident neutron energy spectrum. Intuitively, this makes sense- a continuous function such as $f(E)$ cannot be determined from a finite set of measurements without making further assumptions of the shape of the spectrum. Since the response functions of Bonner spheres overlap over many orders of magnitude and do not have sharp peaks, the measured data do not force convergence to a unique spectrum (Werner 2017). Thus, an unfolding algorithm is needed.

The response functions of the spheres to monoenergetic neutron energies ranging from 2.5×10^{-8} MeV (thermal energy) up to 22.3 MeV were created via MCNP modeling and compared to response functions reported by the International Atomic Energy Agency for a similar BSS system (IAEA 2001). The UMG3.3 code (MAXED + GRAVEL) was used with the calculated mono-energetic neutron response functions to unfold the measured spectra using maximum entropy deconvolution. MCNP and UMG3.3 are both provided by the Radiation Safety Information Computational Center (RSICC) at Oak Ridge National Laboratory.

A Ludlum Model 42-5 Neutron Ball Cart (Fig. 8), which consists of six HDPE spheres of increasing diameter, provided seven total measurement bins (bare detector + six moderating spheres). It was paired with a Ludlum Model 2200 Scaler Ratemeter for electronics and counting.

Figure 8. Ludlum Model 42-5 Neutron Ball Cart and Model 2200 Scaler Ratemeter.

Modeling Neutron Spectra and Dose

Monte-Carlo n-particle transport code (MCNP) is a software package provided by Los Alamos National Laboratory (LANL) and made available through the Radiation Safety Information Computational Center (RSICC). At its most basic, the code generates a particle at a location, sends it in a particular direction, tracks the interactions with matter, and eventually terminates that particle. The transport is simulated based on experimentally derived probability density functions; with the runs of many particles (on the order of millions or billions), one obtains an average of the quantity of interest, often fluence, energy distributions, or energy depositions. MCNP has many applications, from shielding calculations, to dosimetry, to criticality calculations

(Werner 2017). A 3-D geometry of the problem space is built by combining surfaces to become bounded cells. All space in the structured universe of the MCNP problem must be uniquely defined by a cell and the material that fills it.

Atilla4MC (SilverFir Software, CA, USA) integrates CAD model assemblies into meshed MCNP geometries, providing a GUI to streamline setup, running, and visualizing MCNP solutions. Spaceclaim V2022R3 (Ansys, USA) was used to generate a CAD model of the geometries of interest.

MAXED Unfolding Code

The MAXED (*max*imum *e*ntropy *d*econvolution) code was obtained from RSICC in the UMG3.3 software package (Oak Ridge National Laboratory). The algorithm was developed for the deconvolution of multisphere neutron spectrometer data, such as measurements from a Bonner sphere system. MAXED requires an initial estimate of the spectrum, then modifies it using new information from a set of measurements to deconvolute (or unfold) the spectrum. For this project, a priori information about the neutron source and surrounding materials that neutrons may interact with were used to model the irradiation setup and obtain the initial estimate of the spectrum, henceforth called the default spectrum.

The maximum entropy deconvolution can be formulated in discrete terms. For a BSS system with *m* spheres, a neutron energy bin structure is defined with *n* ΔE_k energy bins ($k = 1, \dots, n$ and $n > m$). The continuous response functions $R_i(E)$ and spectrum $f(E)$ from Eq. 4 are replaced with discretized response functions $R_{ik}(E)$ and the discretized spectrum f_k. Then the admissible spectra can be calculated within two restrictions:

$$N_k + \epsilon_k = \Sigma\, R_{ik}\, f_k\, ; i = 1, \ldots, m \quad \text{Eq. 5}$$

$$\Sigma \frac{\epsilon_k^2}{\sigma_k^2} = \Omega \quad \text{Eq. 6}$$

Where:

N_k = the measurements,

σ_k = the standard deviations, and

Ω= the chi-squared statistic.

Ω is typically set equal to the number of detectors. Equation 6 assumes that the measurement uncertainties are normally distributed with zero mean and variances σ_k^2, and is a constraint for handling the unknown uncertainties ϵ_k. Then, the code performs a simulated annealing global optimization method to pick the "best estimate" spectrum from the initial default spectrum and allowable spectra based on the measurements (Reginatto and Goldhagen 1999).

Neutron Sources

A Plutonium-Beryllium (PuBe) neutron source is an alpha-neutron source that produces neutrons through the reaction:

$$\alpha + {}^{9}\mathrm{Be} \rightarrow \mathrm{n} + {}^{12}\mathrm{C}^{*}$$

The α-particle is emitted by the decay of ^{239}Pu to ^{235}U, with a half-life of 24110 y. Impurities of other plutonium isotopes can affect the neutron yield, so, if possible, it is desired to know the isotopic concentrations of the Pu used. The CSU PuBe Howitzer is a 5 Ci (6.5 x 10^6 n/s yield) source (Model NH-3 Neutron Howitzer, Nuclear Chicago Corporation). The howitzer is made up of the 5 Ci source attached to the end of a polyethylene stick, stored in a 50-gallon drum filled with paraffin for neutron shielding. The PuBe source is a mix of ^{239}Pu (half-life: 24,110 years) and ^{9}Be

(stable). PuBe sources have an average neutron energy of 4.3 MeV and a maximum neutron energy of 11 MeV, and the gamma dose rate is 10% of the neutron dose rate. (NRC 2010).

^{252}Cf, another well-known neutron source, decays via spontaneous fission in 3.09% of the total decays, with the other 96.91% of decays by alpha emission. The half-life of ^{252}Cf sources is a relatively short 2.64 y. For all decays, ^{252}Cf has a specific activity of 0.536 mCi μg^{-1} (Martin et al. 1999). CSU procured 80.72 μg in February 2023 for a total starting activity of the source of 43.3 mCi (1.60 GBq). A ^{252}Cf spectrum follows an approximate Watt distribution, similar to the energy distribution of fission neutrons released during nuclear fission. Thus, ^{252}Cf is often used as a proxy neutron source for reactor experiments. The CSU Blockhouse ^{252}Cf source has two experimental states: an unshielded source in which the gamma dose rate is 33% of the neutron dose rate, and a lead shield configuration in which the gamma dose rate is less than 10% of the neutron dose rate (Borak et al. 2019). All experiments in this project were performed with the lead shield off.

Specific Aims

This project aimed to investigate the responses of an alanine-based dosimetry system to multiple types of radiation, radiation dose rates, and radiation doses. The development phase of the proposal had the following specific aims and hypotheses:

1. Development phase
    1.1. Determination of spectrum and dose rates in all neutron sources at CSU (PuBe, ^{252}Cf) using Bonner Sphere Spectrometry and MAXED unfolding.
    1.2. Determination of bare-alanine EPR dose calibration curves for the gamma irradiation facility at CSU (^{137}Cs source).
    1.3. Determination of bare-alanine EPR dose calibration curves for the neutron irradiation facilities at CSU (PuBe, ^{252}Cf). Neutron spectrum, possible radiation doses, and radiation dose rates vary at each location.
    1.4. Comparison of bare-alanine EPR response to modeled photons of different energies vs various neutron spectra.
    1.5. Hypothesis: The neutron spectra will follow literature source spectra with more slowed-down neutrons due to the high-scatter environments.
    1.6. Hypothesis: Bare alanine^{137}Cs will have highest dose-response due to higher photon sensitivity, followed by PuBe source due to higher average neutron energy, ^{252}Cf lowest dose-response due to lowest average neutron energy.

Following the development of the calibration curves for bare alanine, the research phase of the project had the following specific aims:

2. Research phase.

    2.1. Development of an alanine+ filter holder for irradiation integrity.

    2.2. Neutron irradiation and development of dose-response curves of filtered alanine pellets, to target and increase the alanine response to specific neutron energy ranges. Specifically, the filters included:

        2.2.1. ^{113}Cd,

        2.2.2. Gd.

    2.3. Comparison of dose-response curves to calibration curves set up in phase 1.

    2.4. Development of a dosimetry system for specific neutron sources, using bare alanine and alanine filters to allow for concurrent dosimetry during future irradiation studies.

    2.5. Hypothesis: Cd will linearly increase thermal neutron response compared to bare alanine due to secondary photon component. Gd will linearly increase thermal neutron response compared to bare alanine due to secondary Auger electron component, but less than Cd due to the shorter path of Auger electrons compared to Cd.

Methods

Alanine Irradiations and EPR Spectrometer

Alanine pellets were procured from GEX Corporation (Aerial CRT pellets, 4mm diameter, 2.3mm height, 36.5 mg $\pm$ 0.2 mg). A Bruker ELEXSYS 500 X-Band spectrometer (Bruker BioSpin) in the CSU Analytical Resource Center (ARC) was used for the measurements. The Xepr software (Version2.6b.175, 2018) was used to provide the first derivative of the spectrum and subsequent spectrum analysis. A quartz EPR sample tube with low background signal was used, and the background signal of an unirradiated pellet and the tube was measured and subtracted from all measurements. Table 2 shows the EPR settings. For statistical purposes, the measurement of each sample was performed three times.

Table 2. EPR Measurement Spectrometer settings.

Parameter	Value
HF Modulation Frequency	100 kHz
Amplitude of HF modulation	3 G
Microwave power	0.6325 mW
Microwave attenuation	25 dB
Receiver gain	60 dB
Conversion time	5.12 ms
Number of points	1024
Sweep time	5.12 s
Number of scans	40
Total recording time	3.5 min
Central field	3480 G
Sweep field	200 G

The amplitude of the main peak of the alanine spectrum was determined using the Peak Picking function of the xEPR software to identify the maximum and minimum values. The

amplitude was calculated in Excel, and the background signal of the unirradiated alanine pellet was subtracted from each measurement.

A dosimeter was designed to accommodate up to 12 pellets and four signal enhancement foils at a time (Fig. 9). Due to dose rate requirements, some irradiations were performed very close to the source, and only one or two rows used.

Figure 9. Picture of alanine dosimeter holder; (a) open, with foil holder, (b) closed.

Statistical Methods

This research was interested in two independent variables: the radiation source spectrum (^{137}Cs gamma source, PuBe neutron source, and ^{252}Cf neutron+gamma source), as well as the alanine pellet condition (bare alanine, cadmium-filtered, and gadolinium-filtered), and one dependent variable: the EPR response of the alanine pellet (the amplitude of the main EPR peak). Welch's T-test can be used to compare the linear regression models between the experimental conditions and statistically determine if the slopes of the regression models are different, and thus if the relationship between the independent and dependent variables are statistically significantly different. Welch's T-test allows the variances of the groups to be unequal, as it adjusts for the heterogeneity in variance. Welch's T-test is calculated as:

Eq. 7

$$t = \frac{\overline{x_1} - \overline{\overline{x_2}} - d}{\sqrt{\frac{s_1^2}{n_1} + \frac{s_2^2}{n_2}}}$$

$$df = \frac{\left(\frac{s_1^2}{n_1} + \frac{s_2^2}{n_2}\right)^2}{\frac{s_1^4}{n_1^2(n_1 - 1)} + \frac{s_2^4}{n_2^2(n_2 - 1)}} \qquad \text{Eq. 8}$$

Where:

$t =$ test statistic, compared to *t*- distribution;

$\overline{x_i} =$ *i*th sample mean;

s_i = *i*th standard uncertainty (the corrected sample standard deviation divided by the square root of the sample size);

$n_i =$ sample size of *i*th group;

df = degrees of freedom, used with *t*- distribution.

The hypothesis test is expressed as:

- Null Hypothesis (H_0): The slopes of the compared groups are equal ($\beta 1 = \beta 2$).
- Alternative Hypothesis (H_1): The slopes of the compared groups are different ($\beta 1 \neq \beta 2$).

An R function was created to use one of the experimental conditions as the reference model, then performs a Welch's T-test to check if the slopes of the other conditions are statistically significantly different: i.e., outside two standard deviations, from the reference model. The t-value is the number of standard deviations away from reference experiment slope, and the p-value is the traditional test for statistical significance.

Results

BSS Response Functions

The Ludlum Model 42-5 Bonner Sphere System was modeled in MCNP as a 96% enriched ^{6}Li-I crystal surrounded by HDPE spheres of increasing diameter (2, 3, 5, 8, 10, 12 in.) (Fig. 10). When a sphere was not in use, the MCNP cell was instead filled with air. The PMT was modeled as Plexiglass, and the casings were aluminum filled with air (Fig. 11). An F4 tally with an E/EM card of the ENDF/B-VII.1 ^{6}Li(n,t)^{4}He reaction cross section (Chadwick et al. 2011) was used to model the detector response to 56 neutron energies (0.025 eV to 22.3 MeV) in the LiI crystal. The source was a plane-parallel source the size of the largest sphere, emitting monoenergetic neutrons towards the BS system. 5x10^{7} particles were sampled to obtain relative uncertainties less than 0.05.

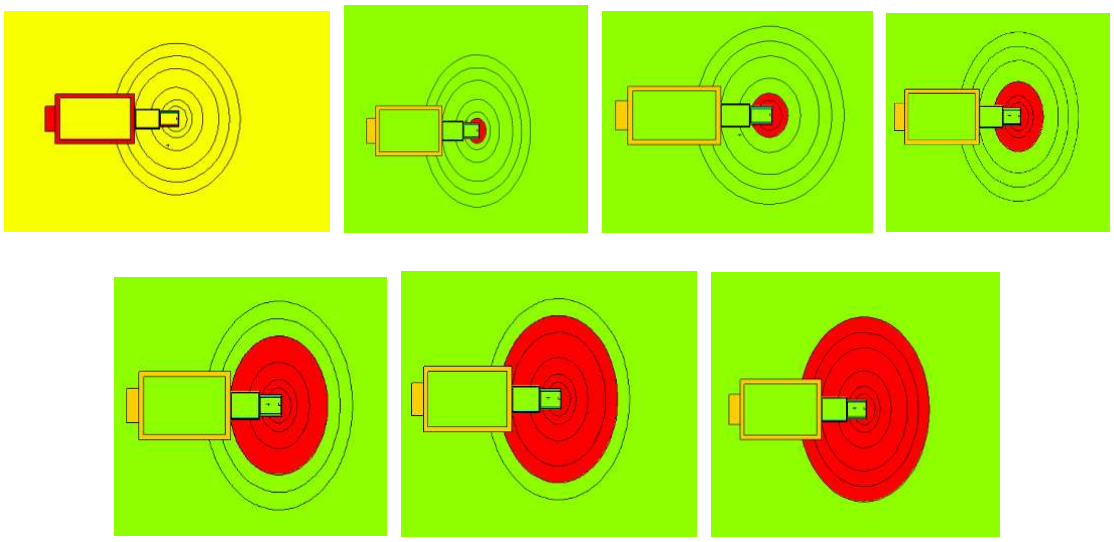

Figure 10. MCNP Model of Bonner Sphere system, bare detector to 12 in Bonner Sphere.

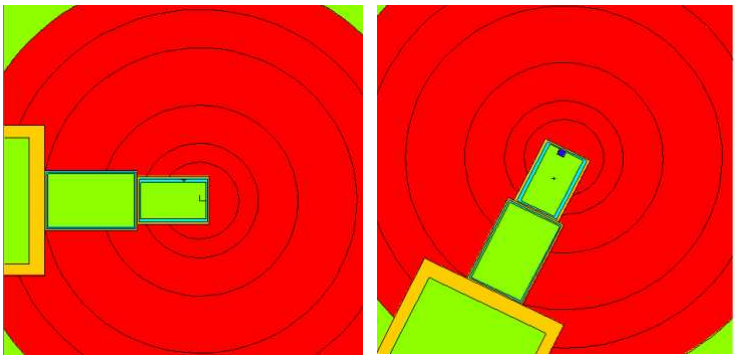

Figure 11. MCNP Model of 12 in. Bonner Sphere system, rotated.

The response functions are shown in Figure 12.

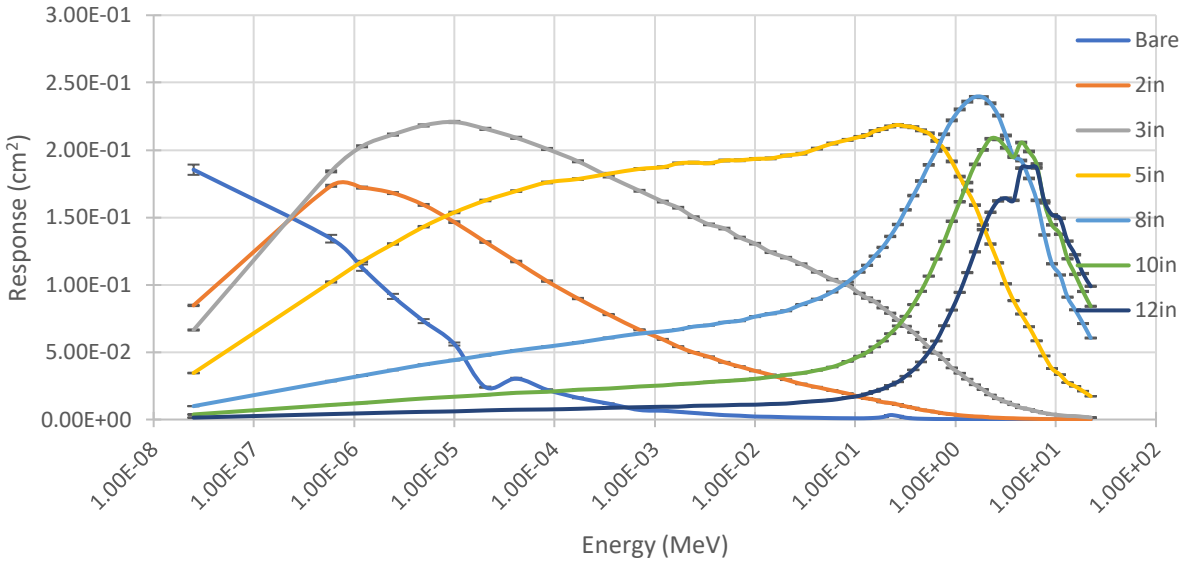

Figure 12. MCNP Modeled Bonner Sphere Response functions with uncertainties at one standard deviation.

BSS Unfolding of ^{252}Cf

The CSU Blockhouse procured 80.72 ug of ^{252}Cf in 2023. The source is contained in a panoramic irradiator located in a concrete shielded vault. A removable lead shield had been used to reduce the gamma dose with minimal change to the neutron dose (Borak et al. 2019). Bonner

sphere measurements were taken at three locations (63 cm, 81 cm, 139 cm from the irradiator tower) in the CSU Blockhouse while the lead gamma shield was surrounding the source, and one location (138 cm from the irradiator tower) with the gamma shield removed. A ^{252}Cf spectrum was taken from the literature as the default spectrum, and scaled for the distance from the source (IAEA 2001). For the deconvolution, the σ_k were set equal to the square roots of the measured number of counts N_k and ranged from 0.5% to 1% of the N_k. To obtain total fluence at each location, the resulting unfolded spectrum was scaled by a constant that minimized the chi-square value of the unfolding in MAXED. The unfolded spectra of the three locations with the lead shield are shown in Figure 13.

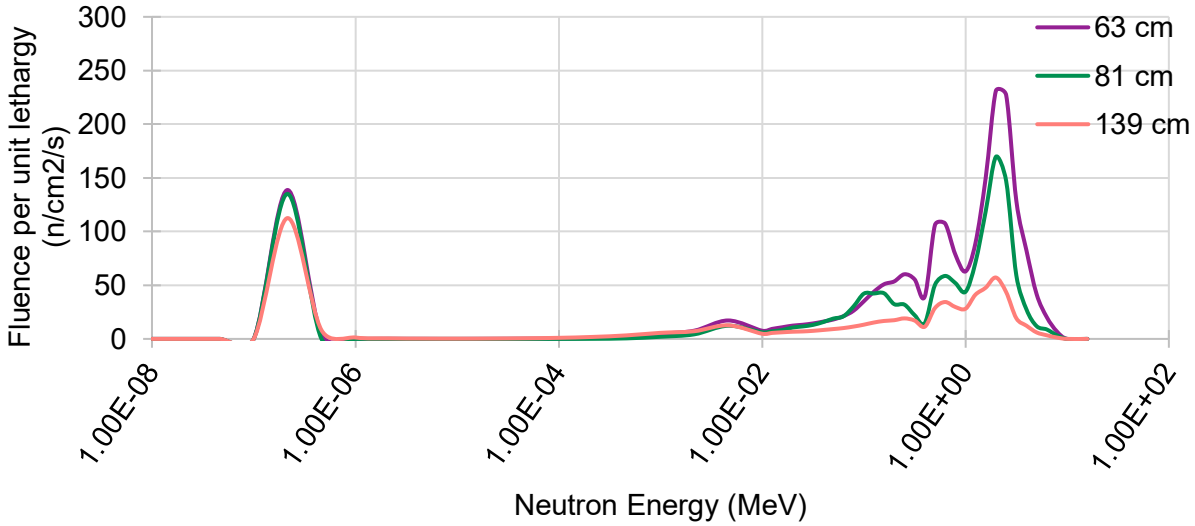

Figure 13. ^{252}Cf Spectra in the CSU blockhouse at three locations from the irradiator tower, with the gamma shield on.

The spectra for the similar locations (138-139 cm from irradiation tower) with and without the lead shield are shown in Figure 14.

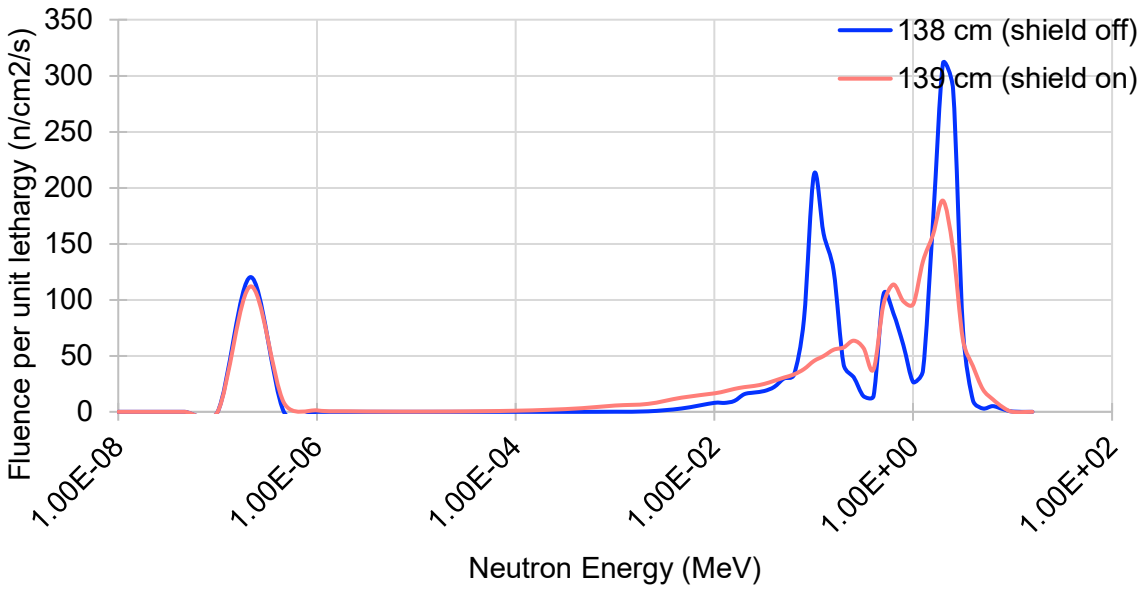

Figure 14. ^{252}Cf neutron spectra in the CSU blockhouse at 138 cm from the irradiator tower with the gamma shield off and 139 cm from the irradiator tower with the gamma shield off.

Due to the dose quantity of interest at the Blockhouse, the ANSI/HPS N13.3 fluence-to-absorbed dose conversion factors (ANSI/HPS 2013) were used to calculate the absorbed dose at each location of interest (Table 3).

Table 3. Absorbed dose rates at BSS measurement locations of the ^{252}Cf source in the CSU Blockhouse.

Distance from Irradiator Tower	Dose rate (mGy/h)
63 cm (shield on)	1.49E-01
81 cm (shield on)	9.11E-02
139 cm (shield on)	3.90E-02
138 cm (shield off)	4.27E-02

The inverse square law was used to calculate the distance and time needed to irradiate a sample to 0.5 Gy, 1 Gy, and 5 Gy (Table 4). Due to concurrent experiments occurring with the source, full

day irradiations were not possible. Therefore, dose for each day was calculated according to the reported exposure time, and decay corrections were applied to the dose rate each week. Additionally, all exposures were taken with the gamma shield off.

Table 4. Irradiation distance and time calculations for neutron absorbed doses in the ^{252}Cf source in the CSU Blockhouse (decay corrected to the starting date of irradiations).

Distance from Irradiator Tower	Dose rate (Gy/h)	Days to 0.5 Gy	Days to 1 Gy	Days to 5 Gy
100 cm	8.14E-05	2.56E+02	5.12E+02	2.56E+03
50 cm	3.26E-04	6.40E+01	1.28E+02	6.40E+02
25 cm	1.30E-03	1.60E+01	3.20E+01	1.60E+02
10 cm	8.14E-03	2.56E+00	5.12E+00	2.56E+01
3 cm	9.04E-02	2.30E-01	4.61E-01	2.30E+00

Literature resources were used to obtain the gamma spectrum of the ^{252}Cf source (Fig. 15) (Czakoj et al. 2024). 96% of the photons produced are below 3 MeV, with 63% below 1 MeV and 36% below 500 keV.

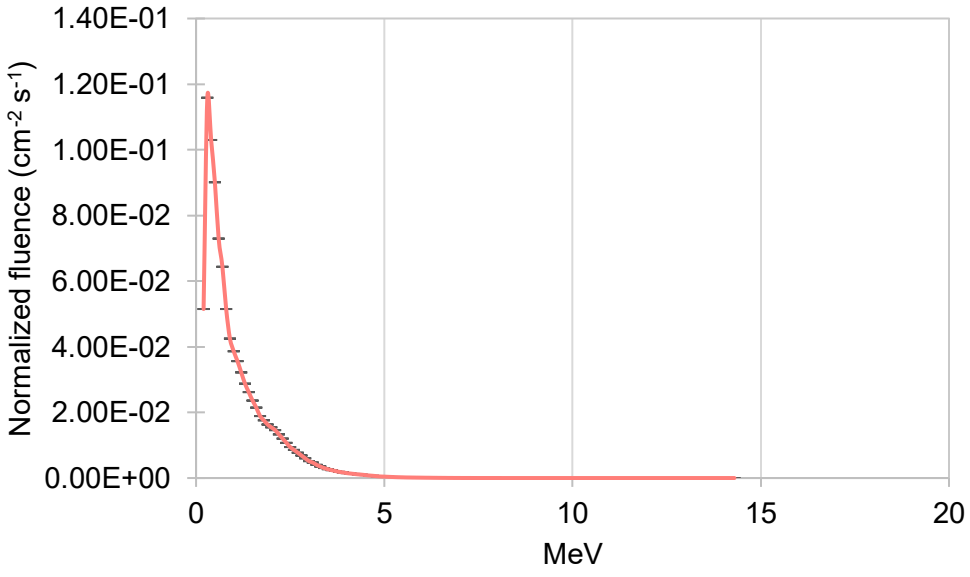

(a)

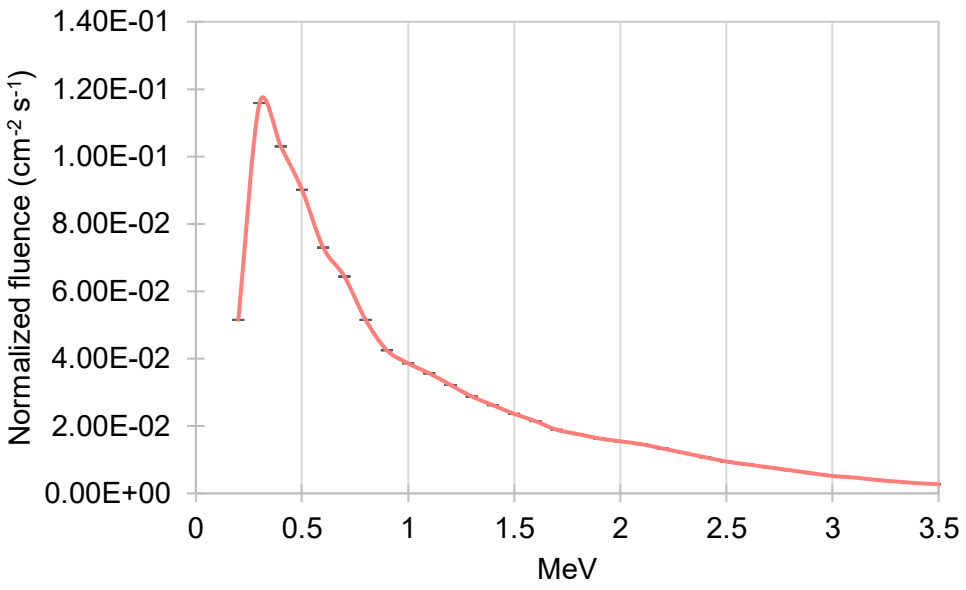

(b)

Figure 15. ^{252}Cf Total Fission Gamma Spectrum, (a) 0- 15 MeV, (b) 0-3.5 MeV (Czakoj et al. 2024).

BSS Unfolding of Plutonium-Beryllium Source

Bonner Sphere Spectrometry was performed in April 2024 for the 5 Ci PuBe Source. Measurements were made at 1 m distance from the unshielded source in MRB 002 (Fig. 16). For the deconvolution, the σ_k were set equal to the square roots of the measured number of counts N_k and ranged from 0.6% to 2% of the N_k. A default PuBe neutron spectrum was taken from the literature (IAEA TRS 403) (Fig. 17), and the result spectrum was scaled by the constant that minimized the algorithm's chi-squared value. The resulting spectrum had many more moderated peaks than the default spectrum, likely due to scatter in the room and off materials in the room (Fig. 18).

Figure 16. Bonner Sphere system at 1 m distance from unshielded PuBe source in MRB 002.

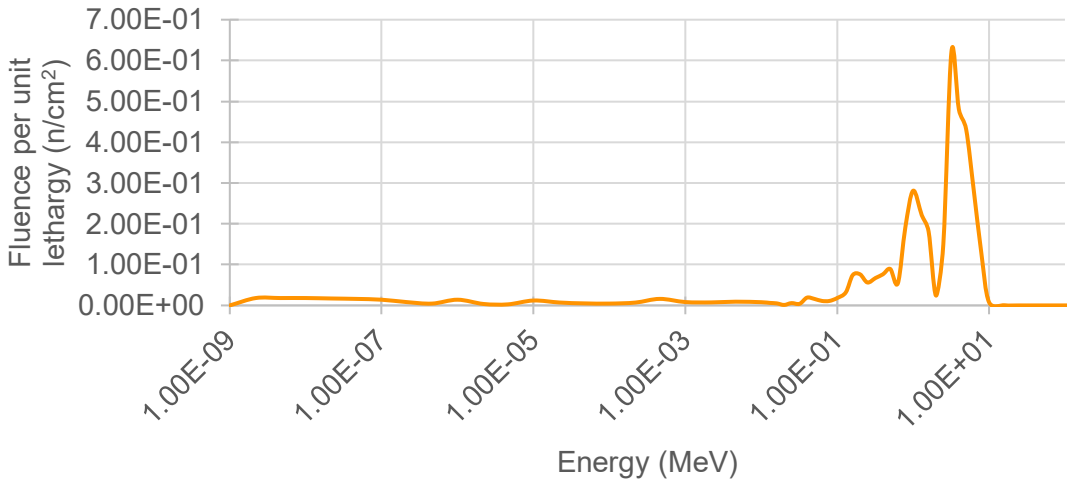

Figure 17. Normalized PuBe Default Spectrum at 1 m (IAEA TRS 403).

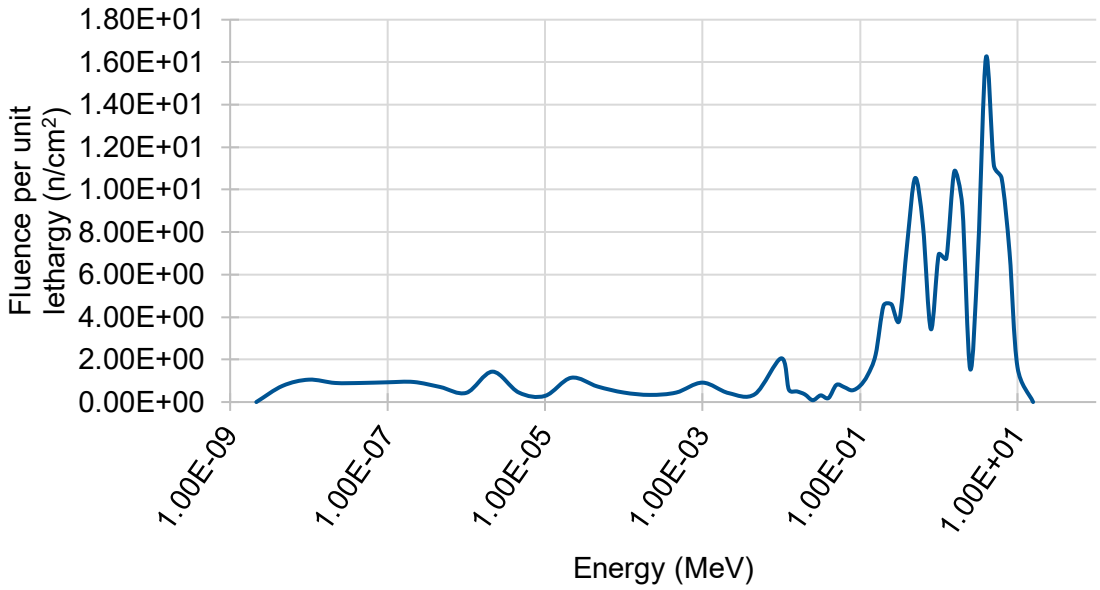

Figure 18. Unfolded PuBe spectrum in MRB 002, 1 m.

ANSI/HPS N13.3 fluence-to-absorbed dose conversion factors (ANSI/HPS 2013) were used to calculate the absorbed dose at each location of interest (Table 5). Although there are thermal peaks, the thermal dose only accounts for $2\pm1\%$ of the total dose, while intermediate and fast neutron account for $3\pm1\%$ and $95\pm1\%$ of the dose, respectively.

Table 5. Absorbed dose rates of the PuBe source at 1m in MRB 002.

Distance (m)	Dose rate (mGy/h)
1	4.42E-02

The inverse square law was used to calculate the distance and time need to irradiate a sample to neutron doses of 0.5 Gy, 1 Gy, and 5 Gy (Table 6). A 5cm distance was chosen for the experiment and a stand was built to allow dosimeter positioning directly in the beamline.

Table 6. Irradiation distance and time calculations for various total absorbed doses in the PuBe source in MRB 002.

Distance from Source	Dose rate (Gy/h)	Days to 0.5 Gy	Days to 1 Gy	Days to 5 Gy
100 cm	4.42E-05	513.49	1026.99	5134.94
30 cm	0.00049	42.46	84.92	424.61
25 cm	0.00071	29.49	58.97	294.87
10 cm	0.00442	4.72	9.44	47.18
5 cm	0.01766	1.18	2.36	11.79

The normalized gamma spectrum of a PuBe source was found in the literature and used as a reference for gamma interactions in alanine. Similar to ^{252}Cf, the majority of photons produced by PuBe sources are 1 MeV or below (Fig. 19).

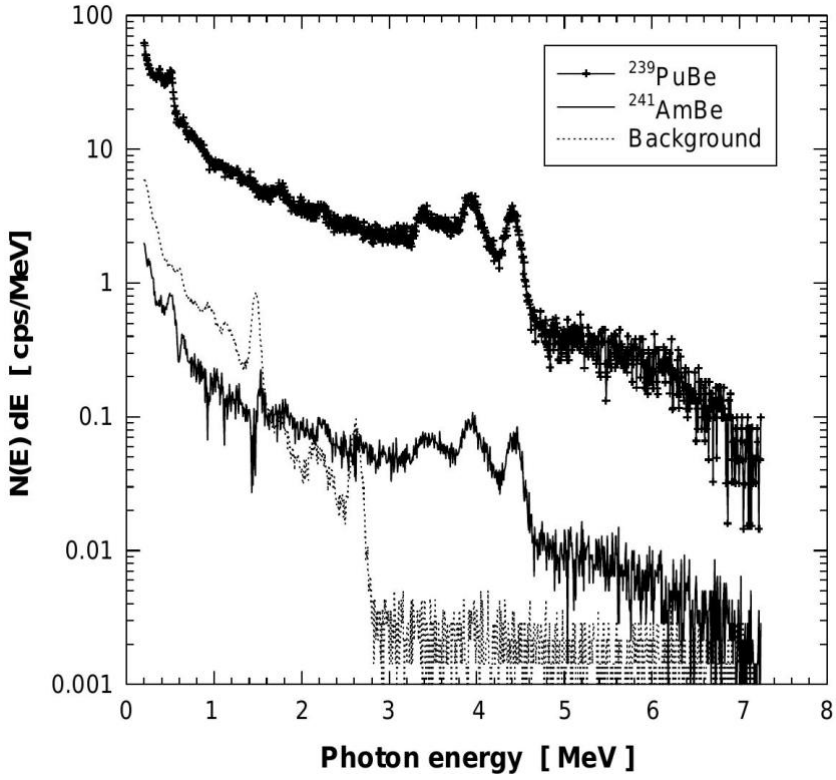

Fig. 19. PuBe, AmBe and background gamma-ray spectra (Vega-Carrillo et al. 2002).

Alanine ^{137}Cs Calibration Curve

Bare alanine pellets (i.e., pellets with no filters) were irradiated in the CSU ^{137}Cs source in MRB Room 006 to doses of 0.5, 1, 3, 5, 8, 10, and 50 Gy. Three pellets were irradiated at each dose point. The background signal of unirradiated pellets was measured in the CSU ARC EPR. Each individual pellet was measured twice with 40 scans. The signal from the three pellets was averaged and background subtracted for the single pellet measurement (Fig. 20). Additionally, three pellets together were measured six times, with two rotations of each ordering of the pellets. The triple-pellet signal was averaged and background subtracted (Fig. 21).

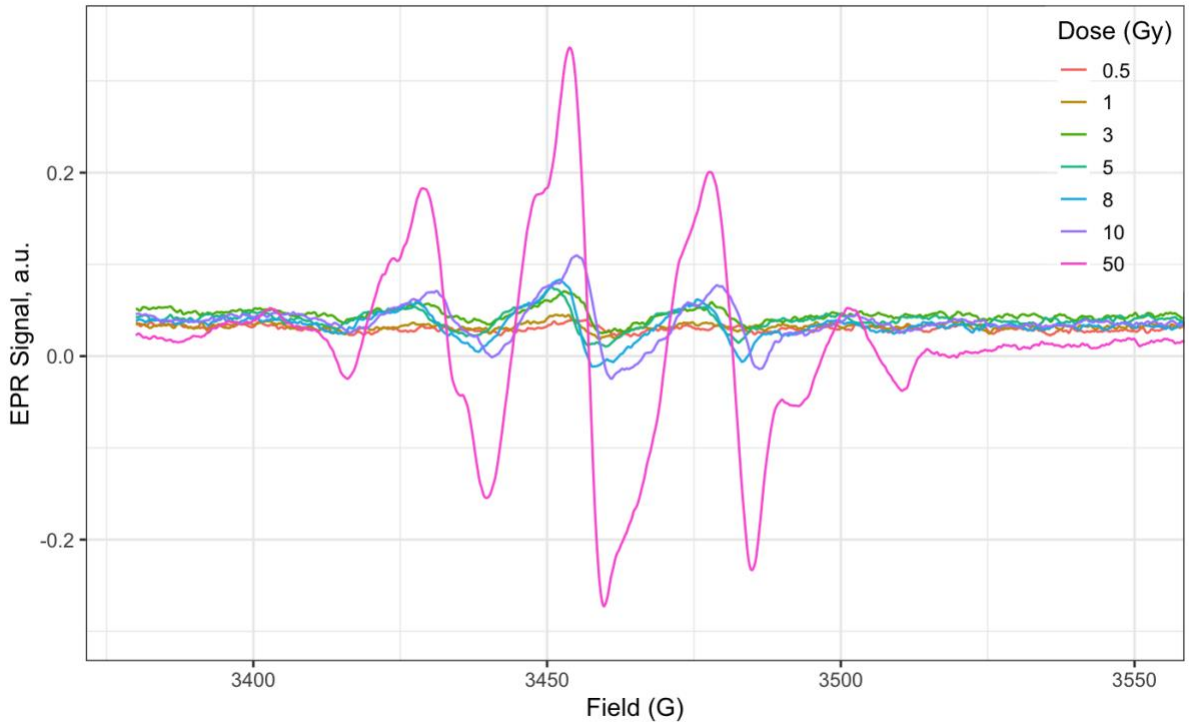

(a)

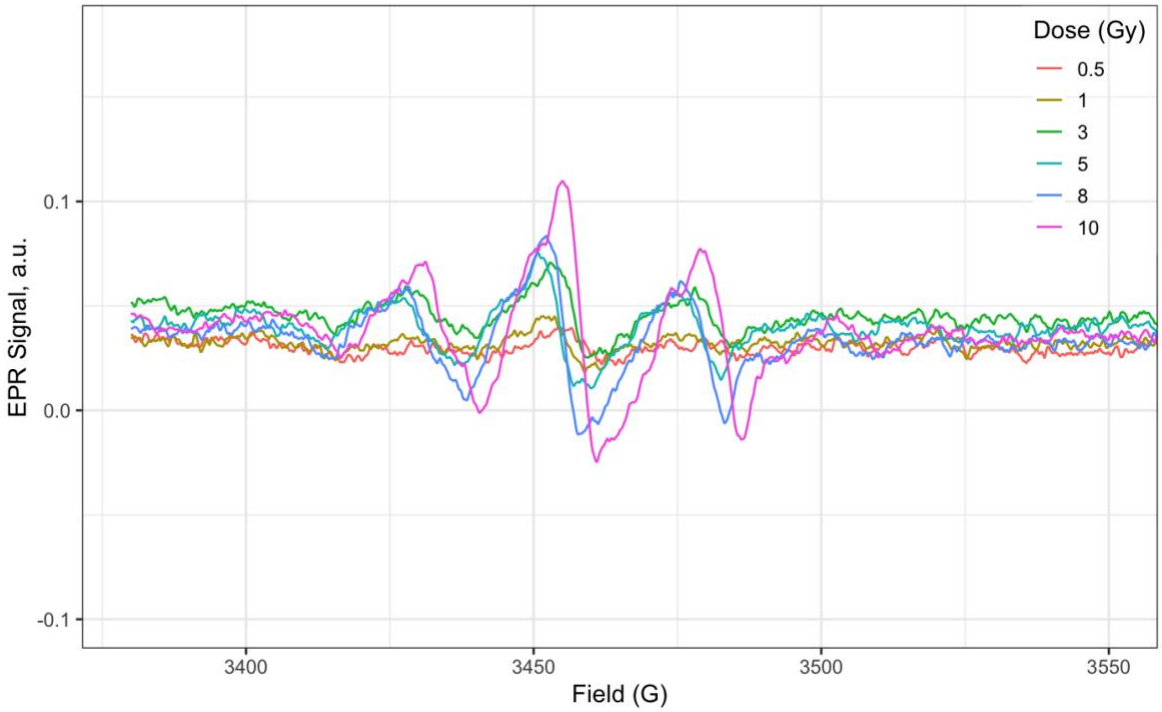

(b)

Figure 20. ^{137}Cs Absorbed dose- Single pellet bare alanine EPR spectrum, (a) 0.5- 50 Gy, (b) 0.5-10 Gy.

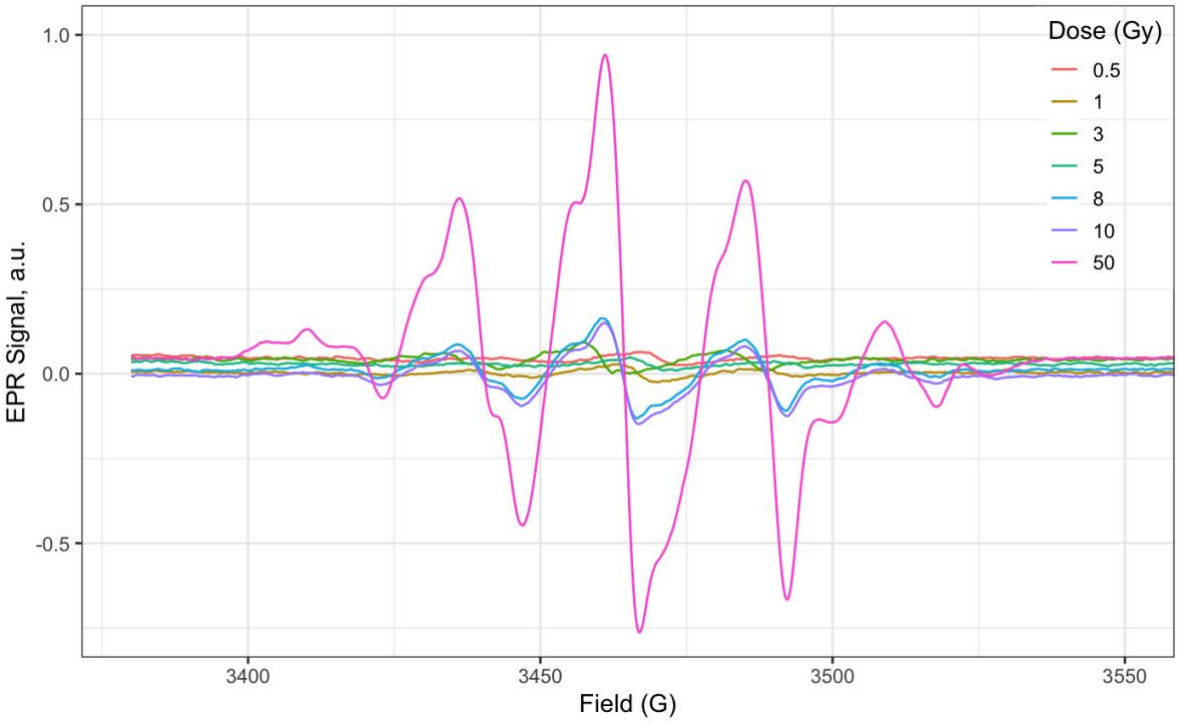

(a)

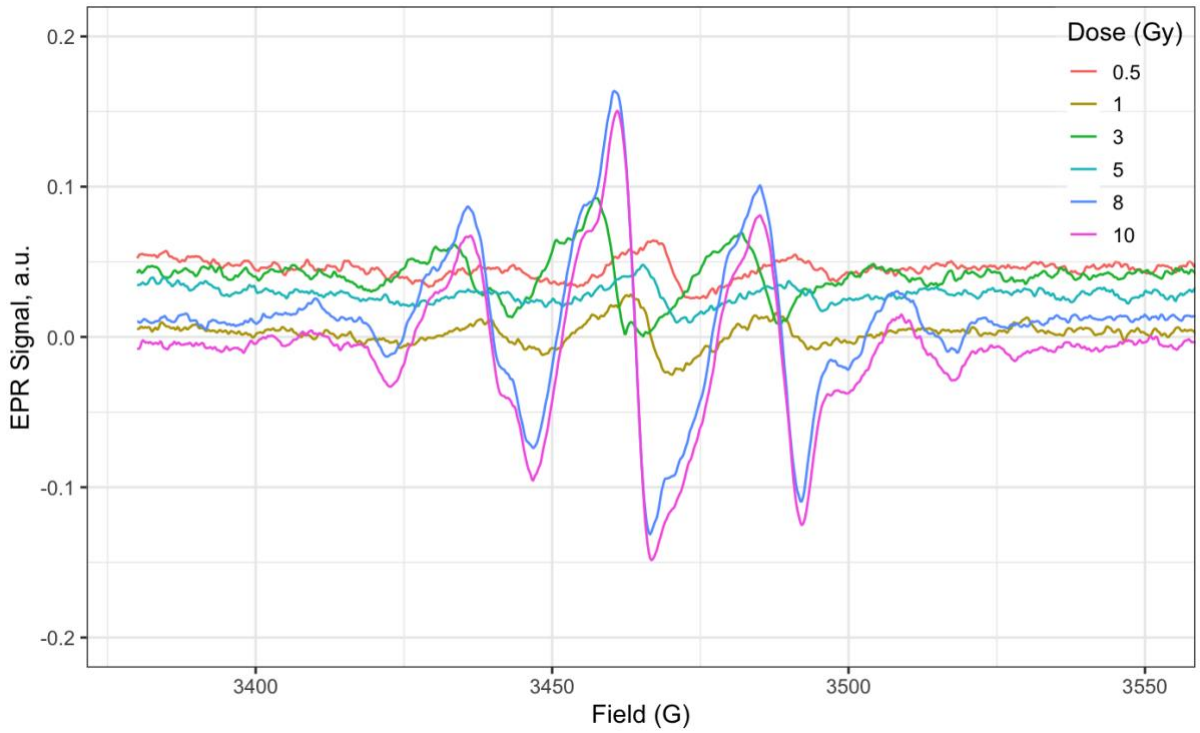

(b)

Figure 21. ^{137}Cs Absorbed dose- Triple pellet bare alanine EPR spectrum, (a) 0.5- 50 Gy, (b) 0.5-10 Gy.

For the single pellet signal, the amplitude of the main alanine radical peak was calculated and averaged between the six measurements (three pellets with two measurements each) at each dose. For the triple pellet signal, the amplitude of the main radical peak was calculated and averaged between six measurements (three permutations of pellets with two measurements each). At low doses (0.5-1 Gy), three times the single pellet amplitude is up to 40% more than the triple pellet amplitude, indicating that the signal is not additive with more mass, or that there is interference in the signal by the increased mass in the resonator. However, as the applied dose increases, the difference between three times the single pellet average and the triple pellet average decreases to 5% at 5 Gy, 3% at 8 Gy, and less than 1% at 10 and 50 Gy (Table 7.)

Table 7. Comparison of ^{137}Cs Bare alanine amplitudes between single pellet and triple pellet.

Dose (Gy)	Single Pellet Average Amplitude	3x Single Pellet Average Amplitude	Triple Pellet Average Amplitude	% Diff (3xSingle vs Triple)
0.5	0.020702	0.062107	0.037430	0.397
1	0.027617	0.082850	0.051254	0.381
3	0.043332	0.129996	0.108872	0.162
5	0.067363	0.202090	0.190705	0.056
8	0.104286	0.312859	0.302232	0.034
10	0.125042	0.375126	0.374051	0.003
50	0.581383	1.744150	1.760810	-0.010

The average amplitudes were plotted and a fit with a linear expression for the creation of a calibration curve (Fig. 22) was generated. The strong linearity of the calibration curves (R^2>0.99) is unsurprising given that the dose range investigated is a very small section of the linear dose-response range (~1 Gy-10^5 Gy) found in the literature.

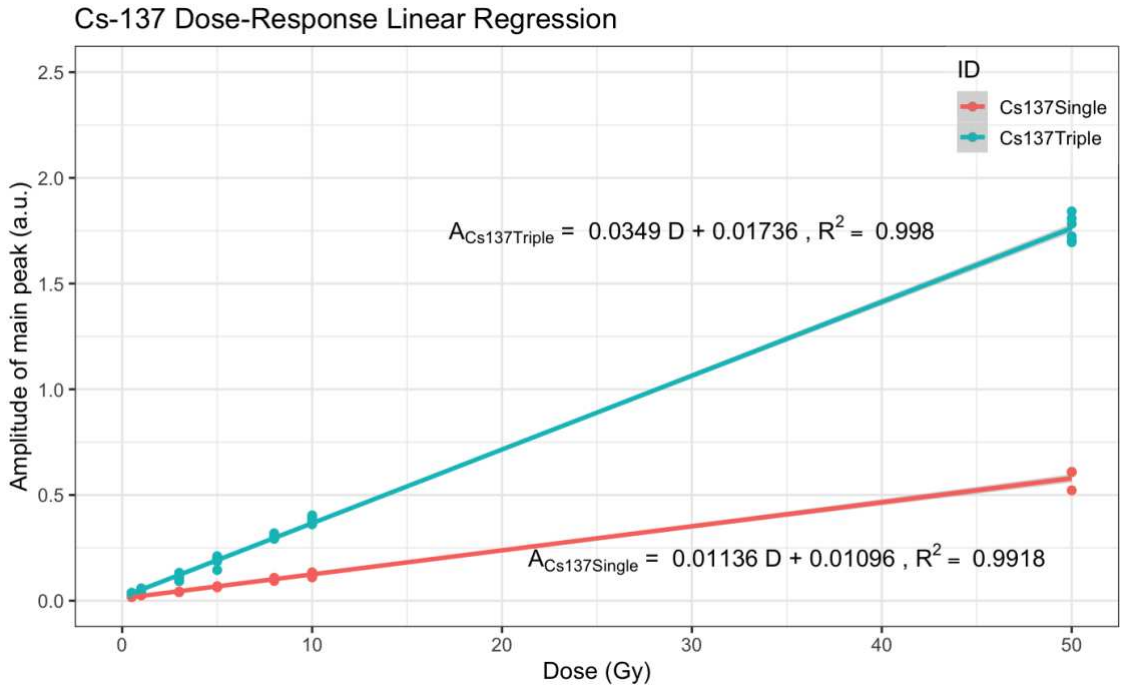

(a)

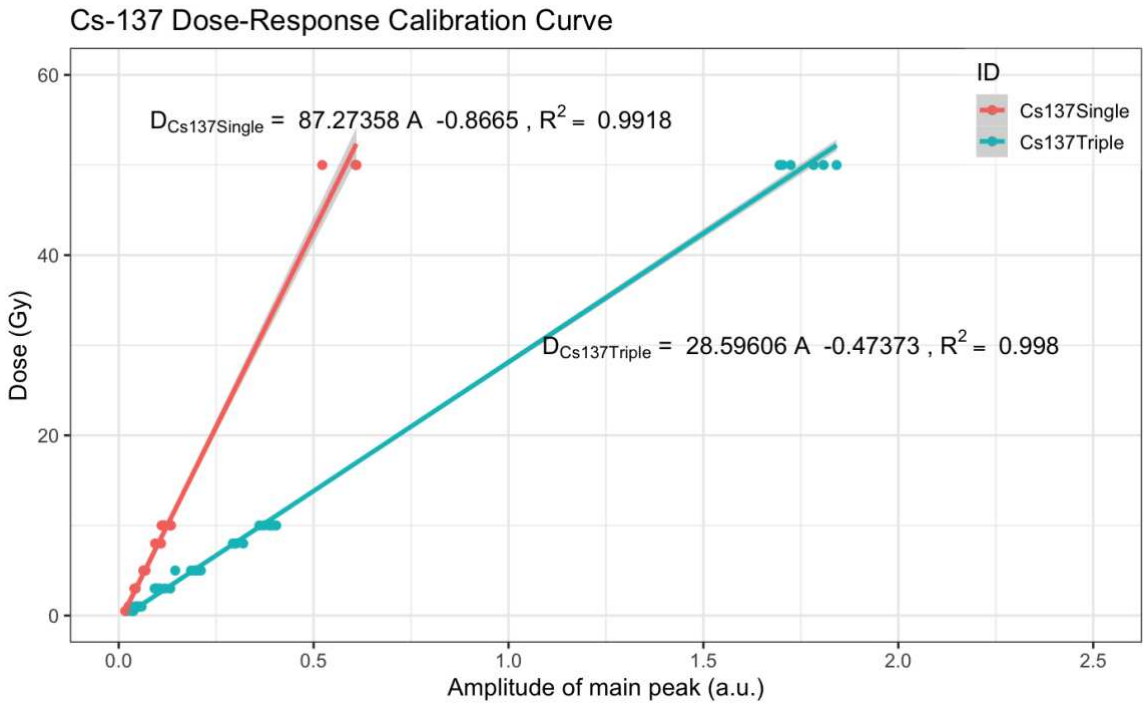

(b)

Figure 22. ^{137}Cs Absorbed Dose- (a) Response Curve and (b) Calibration Curve. 95% confidence interval.

Table 8.

Single pellet calibration curve slope	3x Slope of single pellet	Triple Pellet Slope	% Diff
28.645	85.935	87.988	-0.0233

Three times the single pellet calibration slope is within 3% of the triple pellet calibration curve slope, indicating that across the dose range, the signal is mass-dependent, with little to no loss of signal by increasing the mass of alanine in the resonator.

Neutron Responses

A linear regression was performed on each experimental condition to calculate the condition-specific dose-response relationship (Fig. 23). The Adjusted R^2 value, which takes into account the

sample size of the group, ranged from >0.99 in the ^{137}Cs Single and Triple Pellet regressions, to 0.61 in the single pellet PuBe irradiated, Cadmium filtered group (Table 9). The adjusted R^2 value is consistently larger for the Triple Pellet regression compared to the Single Pellet regression of the same experimental condition, indicating greater linear fidelity with more dosimeter mass.

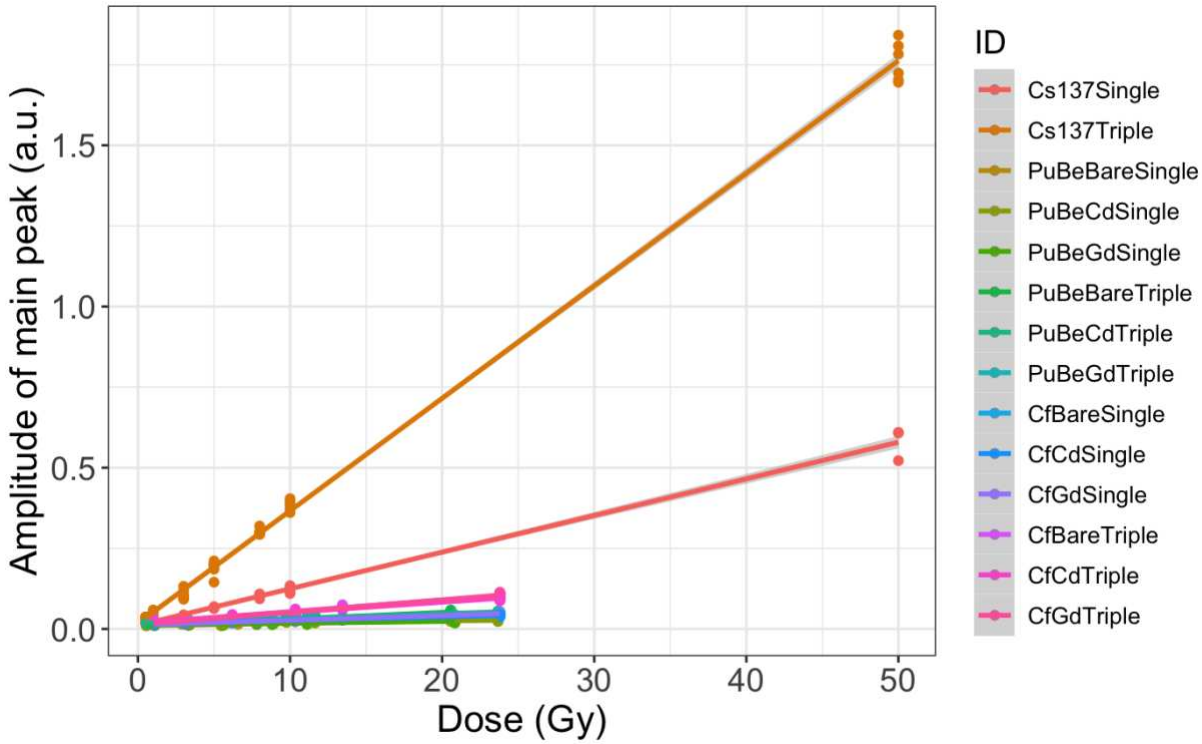

Figure 23. All sources total absorbed dose to amplitude of main peak relationship; linear regression with 95% C.I.

Table 9. Single Pellet linear regression model for all sources and filter conditions.

ID	Pellet Number	Intercept Estimate	Intercept SE	Slope Estimate	Slope SE	Adjusted R^2
Cs137Single	Single	0.0110	0.0041	0.0114	0.0002	0.9914
PuBeBareSingle	Single	0.0101	0.0006	0.0008	0.0000	0.8836
PuBeCdSingle	Single	0.0145	0.0005	0.0005	0.0000	0.7714
PuBeGdSingle	Single	0.0126	0.0006	0.0005	0.0001	0.6184
CfBareSingle	Single	0.0147	0.0007	0.0013	0.0001	0.9058

ID	Pellet Number	Intercept Estimate	Intercept SE	Slope Estimate	Slope SE	Adjusted R^2
CfCdSingle	Single	0.0160	0.0007	0.0011	0.0001	0.9201
CfGdSingle	Single	0.0121	0.0005	0.0015	0.0000	0.9628

Table 10. Triple pellet linear regression models for all sources and filter conditions.

ID	Pellet Number	Intercept Estimate	Intercept SE	Slope Estimate	Slope SE	Adjusted R^2
Cs137Triple	Triple	0.0174	0.0049	0.0349	0.0002	0.9979
PuBeBareTriple	Triple	0.0094	0.0017	0.0021	0.0001	0.9183
PuBeCdTriple	Triple	0.0175	0.0007	0.0015	0.0001	0.9242
PuBeGdTriple	Triple	0.0191	0.0006	0.0009	0.0001	0.8089
CfBareTriple	Triple	0.0176	0.0010	0.0036	0.0001	0.9707
CfCdTriple	Triple	0.0194	0.0011	0.0032	0.0001	0.9745
CfGdTriple	Triple	0.0138	0.0010	0.0038	0.0001	0.9784

The bare alanine conditions for each source are plotted with their linear regressions in Figure 24.

It is visually apparent that the slopes of each condition are distinct.

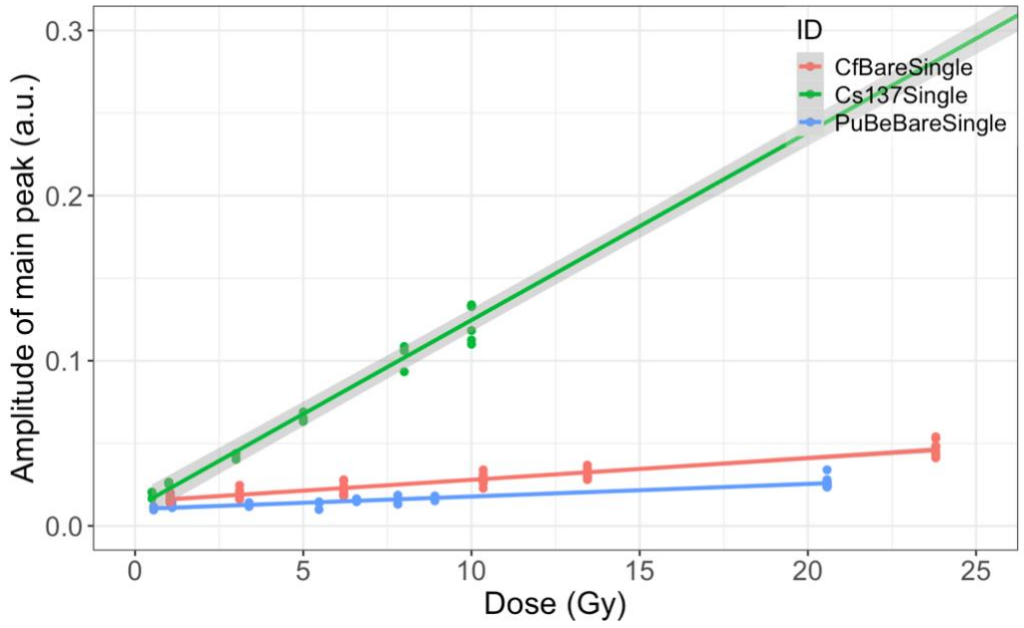

(a)

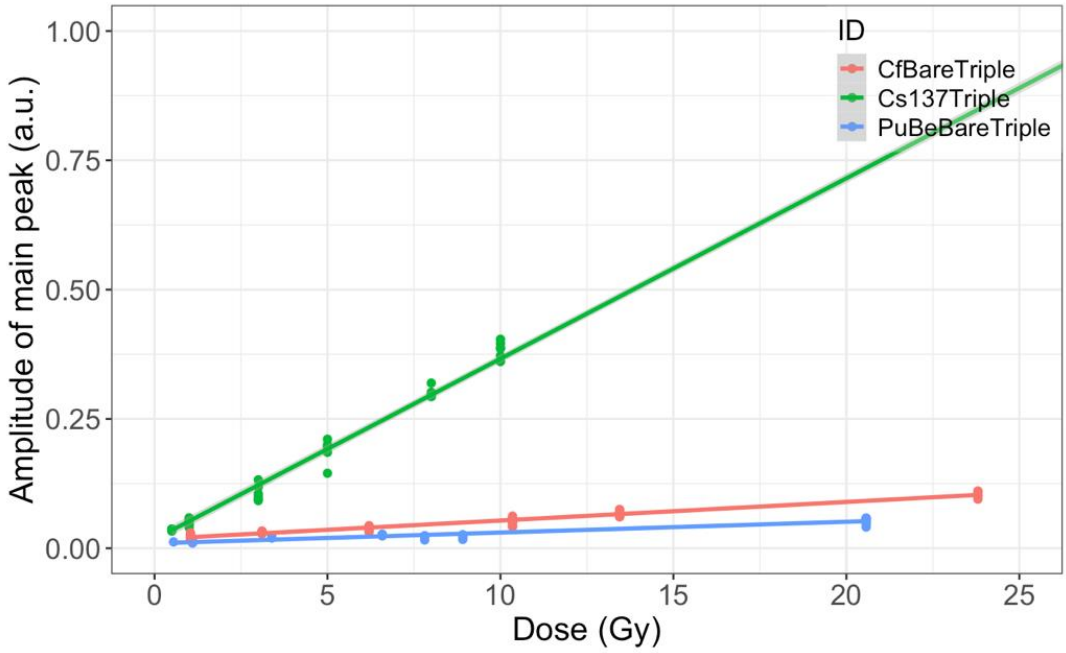

(b)

Figure 24. (a) Bare alanine single pellet linear regression and (b) Bare alanine triple pellet linear regression, 95% confidence interval.

Welch's T-test within the single and triple pellet subsets calculates that the slopes of each radiation source are statistically significantly different with reference to the ^{137}Cs linear

regression (single and triple pellet, respectively), confirming the hypothesis that the radiation source affects the response of the bare alanine dosimeter. Thus, a calibration curve cannot be used interchangeably between radiation sources to obtain dose information, unless the source sensitivity is taken into account.

Table 11. Single Pellet Linear Model Comparison

Term	Estimate	Std. Error	t value	p value	Significance
Intercept	0.0125	0.0011	11.34	2.87e-20	***
Reference: Cs-137 Single Slope	0.0113	0.0001	122.35	3.10e-120	***
PuBeBare Single Slope	-0.0107	0.0001	-77.34	2.21e-98	***
CfBare Single Slope	-0.0099	0.0001	-77.14	2.90e-98	***

***: p<<< 0.001; **:p < 0.001; *: p< 0.01; . : p< 0.05

Table 12. Triple Pellet Linear Model Comparison

Term	Estimate	Std. Error	t value	p value	Significance
Intercept	0.0163	0.0020	8.05	6.16e-13	***
Reference: Cs-137 Triple Slope	0.0349	0.0001	256.61	1.40e-168	***
PuBeBare Triple Slope	-0.0332	0.0002	-133.40	4.75e-134	***
CfBare Triple Slope	-0.0312	0.0002	-139.03	3.17e-136	***

***: p<<< 0.001; **:p < 0.001; *: p< 0.01; . : p< 0.05

Neutron Subset

The neutron sources were isolated to compare the responses to different spectra and identify if the presence of the filters produced a statistically significant response in the alanine pellets. The two different neutron sources are grouped together, with the ^{252}Cf source having a higher total response to the same total dose than the PuBe source (Fig. 25). The ^{252}Cf had a higher gamma contribution, whose influence will be discussed later.

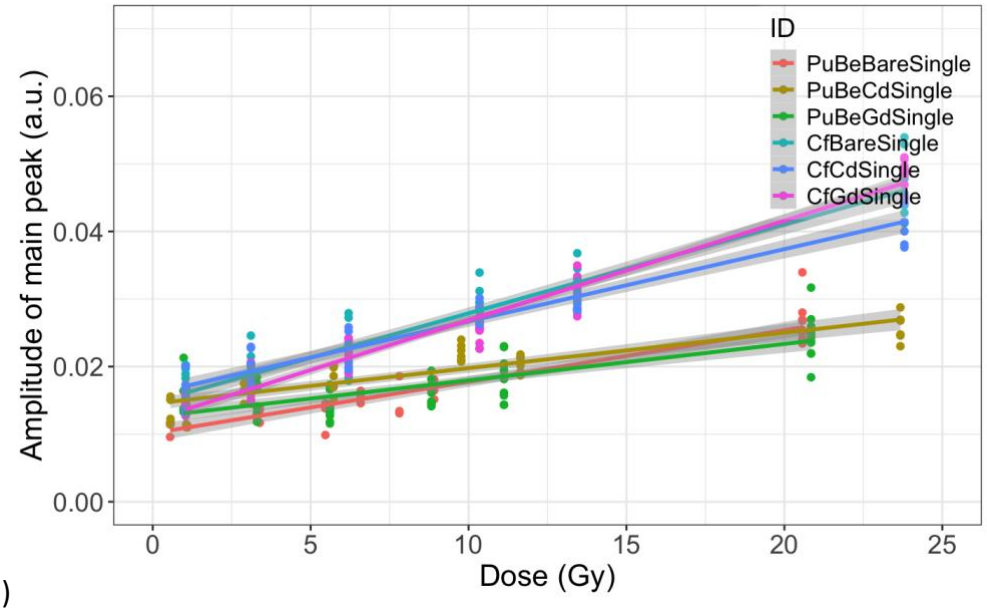

(a)

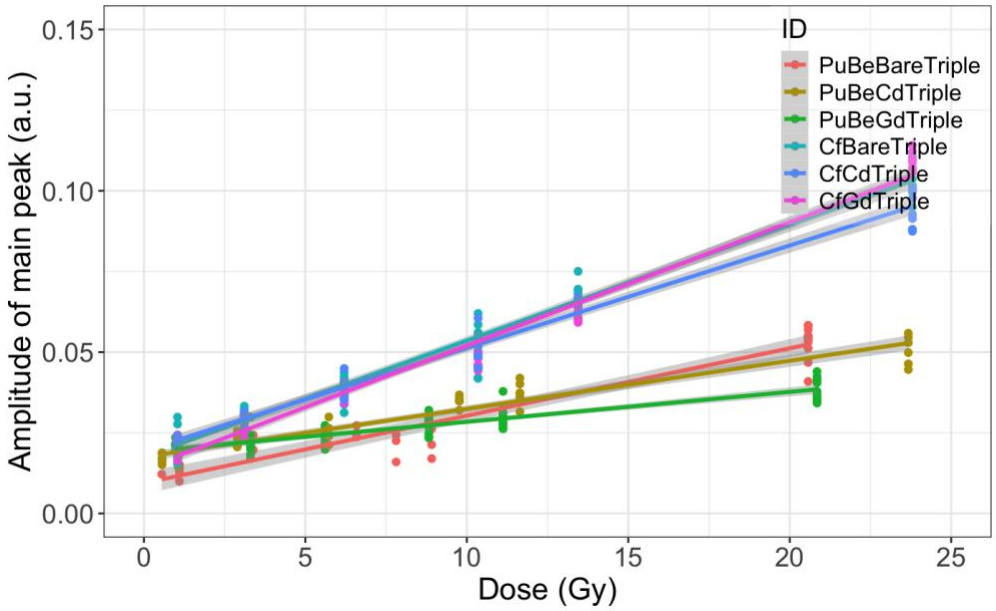

(b)

Figure 25. (a) Single Pellet linear regression for all neutron sources and filter conditions. (b) Triple Pellet linear regression for all neutron sources and filter conditions. 95% confidence interval.

Welch's T-test within the single and triple pellet subsets calculates that the slopes of each radiation source are statistically significantly different with reference to the PuBe Bare

linear regression (single and triple pellet, respectively), confirming the hypothesis that the radiation source and the filter type affects the response of the bare alanine dosimeter (Table 13 and Table 14).

Table 13. Single pellet Welch's T-test for neutron source linear regressions.

Term	Estimate	Std. Error	t value	p value	Significance
Intercept	0.0134	0.0003	50.96	2.75e-144	***
Reference: PuBe Bare Single	0.0006	0.0000	14.04	2.51e-34	***
PuBeGd Single	-0.0001	0.0000	-1.79	7.47e-02	.
PuBeCd Single	0.0000	0.0001	0.67	5.03e-01	
CfBare Single	0.0008	0.0000	17.54	4.55e-47	***
CfGd Single	0.0008	0.0000	17.33	2.64e-46	***
CfCd Single	0.0007	0.0001	12.81	6.61e-30	***

***: p<<< 0.001; **: p < 0.001; *: p< 0.01; . : p< 0.05

Table 14. Triple pellet Welch's T-test for neutron source linear regressions.

Term	Estimate	Std. Error	t value	p value	Significance
Intercept	0.0165	0.0004	38.21	1.11e-110	***
Reference: PuBeBare Triple	0.0017	0.0001	26.73	1.07e-77	***
PuBeGd Triple	-0.0006	0.0001	-7.37	2.16e-12	***
PuBeCd Triple	0.0001	0.0001	0.94	3.49e-01	
CfBare Triple	0.0020	0.0001	26.49	6.28e-77	***
CfGd Triple	0.0020	0.0001	26.26	3.27e-76	***
CfCd Triple	0.0017	0.0001	20.53	5.42e-57	***

***: p<<< 0.001; **: p < 0.001; *: p< 0.01; . : p< 0.05

PuBe Dose-Response

Alanine pellets in the three experimental conditions (bare, gadolinium foil, cadmium foil) were sequentially irradiated in the CSU PuBe source in MRB Room 002 to total absorbed doses of

0.55, 1.1, 3.39, 5.47, 8.91, and 20.57 Gy (neutron absorbed doses of 0.5, 1, 3, 5, 8, and 18.7 Gy). Two sets of three pellets were irradiated as a together. Each individual pellet was measured twice with 40 scans. Additionally, three pellets stacked together were measured six times, with two rotations of each ordering of the pellets. A linear regression was performed and plotted on all conditions (Fig. 26).

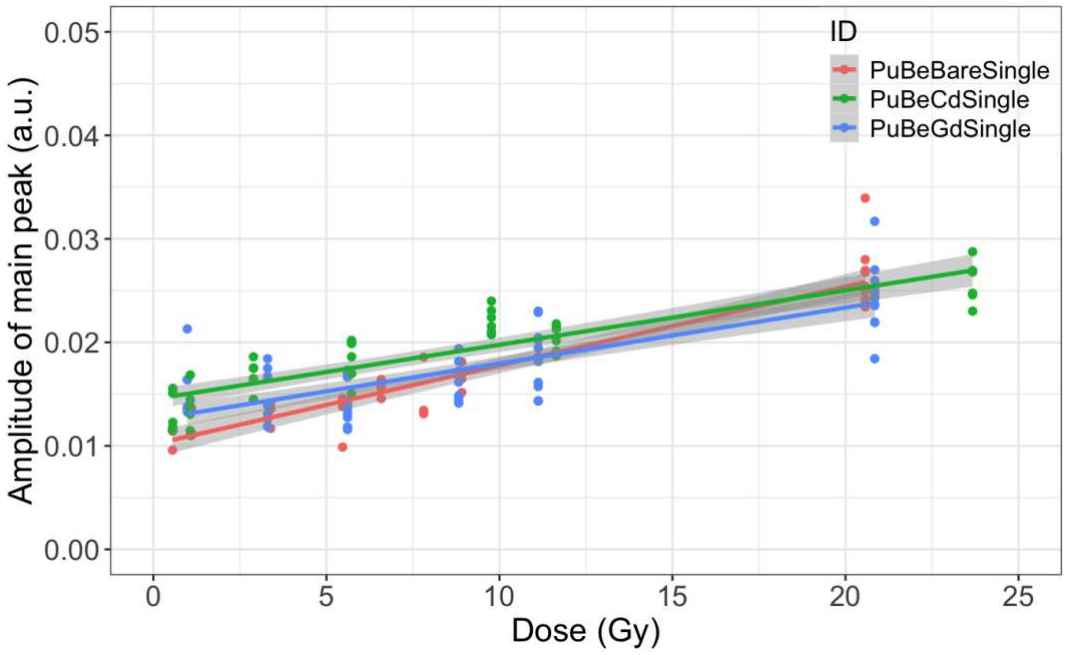

(a)

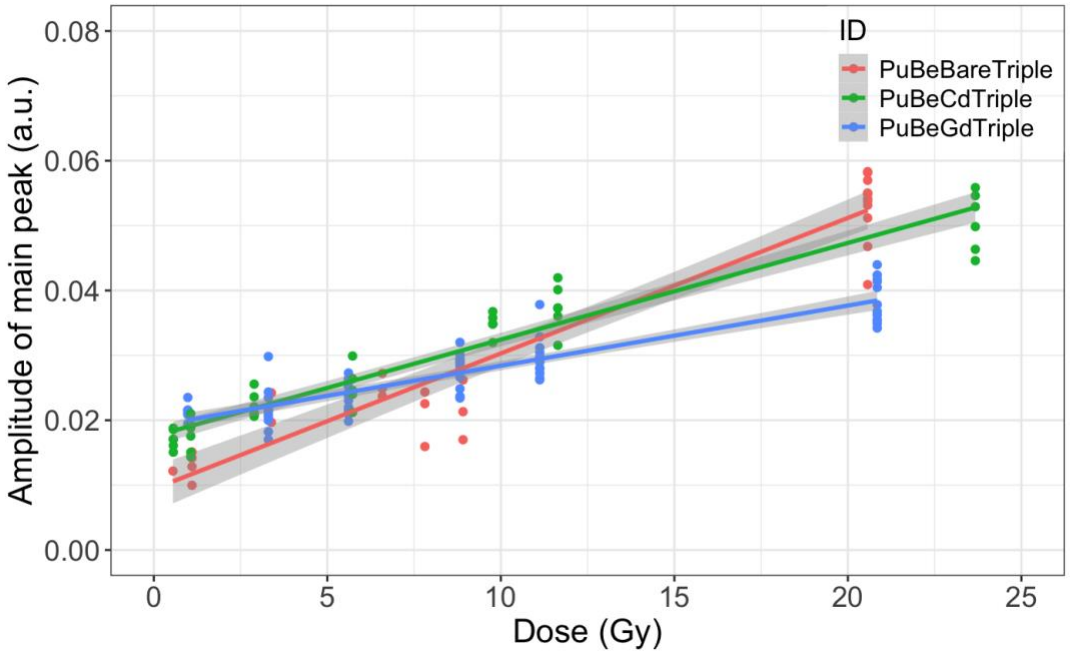

(b)

Fig. 26. (a) Single pellet alanine linear regression in PuBe field, with filters. (b) Triple pellet alanine linear regression in PuBe field, with filters. 95% confidence intervals.

The PuBeCd Single pellet slope is not statistically significantly different from the PuBe Bare Single Pellet slope, but the PuBe Gd slope is statistically significantly different from the bare condition (Table 15). This indicates that the gadolinium foil changes the alanine response. Based on Fig. 26, cadmium raises a single pellet of alanine's response to neutrons until approximately 17 Gy total absorbed dose in a single pellet. However, above 17 Gy, cadmium decreases the alanine response compared to a bare pellet. Therefore, while we should use the linear model for each experimental case to get the best calculation of dose/ amplitude, at lower doses the comparison of the cadmium foil-filtered alanine to the bare alanine may be able to be used to extract additional thermal neutron data. The gadolinium slope is statistically significantly different from the bare alanine slope, and also crosses from increasing the alanine response compared to bare alanine, to decreasing the response compared to bare alanine around 10 Gy.

Similar to the single pellet subset, the PuBe Gd triple pellet slope is statistically significantly different from the PuBe Bare triple pellet slope, but the PuBe Cd slope is not statistically significantly different. Additionally, the PuBe Gd triple pellet response relative to the PuBe Bare triple pellet response varies with respect to the total dose, but changes from increasing the response to decreasing the response at a lower dose than the single pellet subset. That is, the gadolinium foil changes the alanine response by raising its response to neutrons at a lower dose than the single pellets (7 Gy vs 10 Gy) but decreasing its response to neutrons at doses above 7 Gy. Similarly, while the cadmium slope is not statistically significantly different from the bare alanine slope, Figure 26 (b) shows that the overall response is higher for a cadmium-filtered pellet than a bare pellet until 13 Gy, then decreases the alanine response.

Table 15. PuBe Single Pellet Welch's T-test on linear regression models.

Term	Estimate	Std. Error	t value	p value	Significance
Intercept	0.0127	0.0004	35.51	2.74e-71	***
Reference: PuBeBare Single	0.0006	0.0000	14.76	3.55e-30	***
PuBeGd Single	-0.0001	0.0000	-1.69	9.34e-02	.
PuBeCd Single	0.0000	0.0001	0.78	4.37e-01	

***: p<<< 0.001; **: p < 0.001; *: p< 0.01; . : p< 0.05

Table 16. PuBe Triple Pellet Welch's T-test on linear regression models.

Term	Estimate	Std. Error	t value	p value	Significance
Intercept	0.0168	0.0006	28.93	5.41e-59	***
Reference: PuBeBare Triple	0.0017	0.0001	25.86	1.64e-53	***
PuBeGd Triple	-0.0006	0.0001	-7.79	1.70e-12	***
PuBeCd Triple	-0.0001	0.0001	-1.51	1.33e-01	

***: p<<< 0.001; **: p < 0.001; *: p< 0.01; . : p< 0.05

Three times the bare single pellet average amplitude was compared to the triple pellet amplitude (Table 17). At lower doses (0.5- 8.91 Gy), three times the single pellet amplitude is up to 62.8% more than the triple pellet amplitude, indicating that the signal is not additive with more mass, or that there is interference in the signal by the increased mass in the resonator. At 20.57 Gy, three times the single pellet amplitude was 31% more than the triple pellet amplitude (Table 18). This contrasts with the ^{137}Cs average amplitudes, in which the difference between three times the single pellet amplitude was less than 1% different than the average triple pellet amplitude.

Table 18. Bare PuBe single pellet vs triple pellet average amplitudes.

Neutron Dose (Gy)	Single Pellet Average Amplitude	3x Single Pellet Average Amplitude	Triple Pellet Average Amplitude	% Diff (3xSingle vs Triple)
0.55	0.010896	0.032689	0.012167	0.628
1.1	0.011389	0.034167	0.013031	0.619
3.34	0.013100	0.039300	0.021957	0.441
6.58	0.015633	0.046900	0.025269	0.461
7.81	0.015031	0.045093	0.020952	0.535
8.91	0.016573	0.049718	0.021511	0.567
20.57	0.025983	0.077950	0.053604	0.312

Cf Dose-Response

Alanine pellets in the three experimental conditions (bare, gadolinium foil, cadmium foil) were sequentially irradiated in the CSU ^{252}Cf source to total absorbed doses of 1.04, 3.107, 6.201, 10.348, 13.444, and 23.800 Gy (neutron absorbed doses of 0.8, 2.39, 4.77, 7.96, 10.34, and 18.308 Gy). Three sets of three pellets in each condition were irradiated together. Each individual pellet was measured twice with 40 scans. Additionally, three pellets stacked together were measured six times, with two rotations of each ordering of the pellets. A linear regression was performed and plotted on all conditions (Fig. 27).

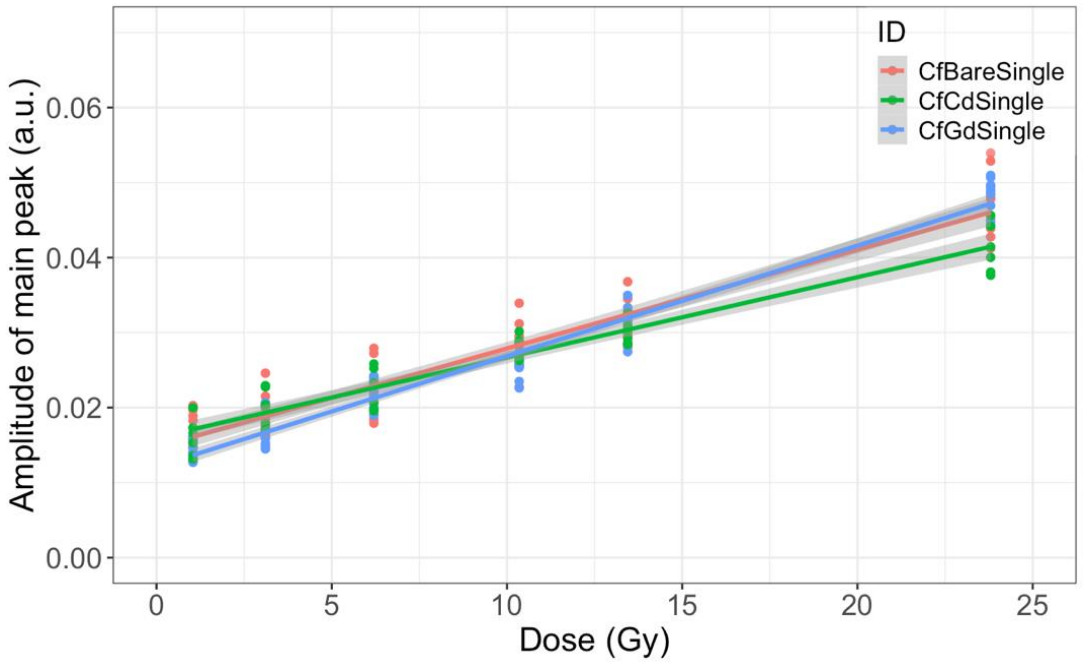

(a)

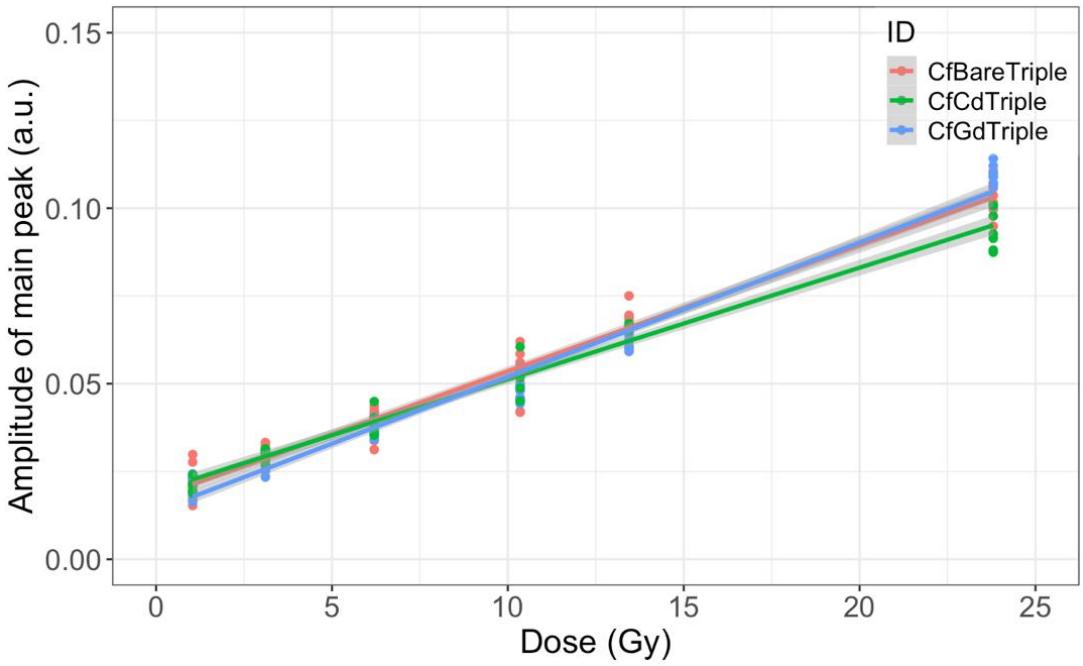

(b)

Figure 27. (a) Single pellet alanine linear regression in ^{252}Cf field, with filters. (b) Triple pellet alanine linear regression in ^{252}Cf field, with filters. 95% confidence intervals.

The CfCd Single pellet slope is statistically significantly different from the Cf Bare Single Pellet slope, but the CfGd Single slope is not (Table 19). This indicates that the cadmium foil

changes the alanine response. Based on Fig. 27, cadmium raises a single pellet of alanine's response to neutrons until approximately 5 Gy total absorbed dose. Above 5 Gy, it lowers the alanine response to the ^{252}Cf field as compared to the bare alanine. While the single pellet gadolinium slope is not statistically significantly different from the bare alanine slope in the ^{252}Cf source, it also crosses from decreasing the response compared to bare alanine, to increasing the response compared to bare alanine around 9 Gy. This is the opposite effect than gadolinium on the PuBe source, in which it first increased the EPR response compared to bare alanine, then decreased it after approximately 7 Gy.

Similar to the single pellet subset, the PuBe Gd triple pellet slope is not statistically significantly different from the PuBe Bare triple pellet slope, but the PuBe Cd slope is statistically significantly different (Table 20). The PuBe Gd triple pellet response relative to the PuBe Bare triple pellet response varies with respect to the total dose, changing from decreasing the response to increasing the response at about the same dose as the single pellet subset. That is, the gadolinium foil changes the alanine response by lowering its response to neutrons until about 9 Gy but increasing its response to neutrons at doses above 9 Gy. The triple pellet cadmium slope is statistically significantly different from the bare alanine slope, and Figure 27(b) shows that the effect changes from increasing to decreasing the alanine response compared to bare alanine at approximately 5 Gy (at the same dose point as the single pellet ^{252}Cf subset).

Table 19. Cf Single Pellet Welch's T-test on linear regression models.

Term	Estimate	Std. Error	t value	p value	Significance
Intercept	0.0141	0.0004	37.27	1.63e-75	***
Reference: CfBare Single	0.0014	0.0000	33.85	3.82e-70	***
CfGd Single	0.0000	0.0000	-0.22	8.29e-01	
CfCd Single	-0.0002	0.0001	-3.29	1.28e-03	**

***: p<<< 0.001; **: p < 0.001; *: p< 0.01; . : p< 0.05

Table 20. Cf Triple Pellet Welch's T-test on linear regression models.

Term	Estimate	Std. Error	t value	p value	Significance
Intercept	0.0167	0.0006	27.13	4.85e-58	***
Reference: CfBare Triple	0.0037	0.0001	56.39	4.25e-99	***
CfGd Triple	0.0000	0.0001	-0.24	8.14e-01	
CfCd Triple	-0.0003	0.0001	-3.66	3.56e-04	***

***: p<<< 0.001; **: p < 0.001; *: p< 0.01; . : p< 0.05

Neutron Sensitivity Calculations

The relative sensitivity of the alanine and alanine+filters in relation to the ^{137}Cs standard source was calculated as the quotient of the dose of the neutron irradiated pellets calculated by the ^{137}Cs calibration ($D_{measured}$) curve minus the known gamma dose (D_γ) divided by the known neutron dose (D_n) (all in Gy):

$$k = \frac{D_{measured} - D_\gamma}{D_n}. \quad \text{Eq. 9}$$

The PuBe conditions have lower relative sensitivities than the ^{252}Cf conditions.

Table 21. Relative sensitivity to neutrons of the alanine experiments.

Experiment	Relative sensitivity to neutrons
PuBe Bare	0.056 ± 0.085
PuBe Gd	0.089 ± 0.129
PuBe Cd	0.137 ± 0.156
Cf Bare	0.245 ± 0.212
Cf Gd	0.191 ± 0.119
Cf Cd	0.218 ± 0.171

Calibration Curves

Calibration curves for each experimental condition were created by reversing the independent and dependent variable in the linear regression (i.e., obtaining a linear regression for dose based on EPR signal response) (Tables 22, 23). The adjusted R^2 values are the same as for the dose-response linear regression. The adjusted R^2 values are larger for the triple pellet conditions than for the single pellet conditions, indicating greater linear fidelity with more dosimeter mass. Additionally, the ^{252}Cf experiments had larger adjusted R^2 values than the PuBe experiments.

Table 22. Calibration Curve linear regressions for all single pellet alanine conditions.

ID	Intercept Estimate	Intercept SE	Slope Estimate	Slope SE	Adjusted R^2
Cs137Single	-0.8665	0.3722	87.2736	1.6939	0.9914
PuBeBareSingle	-10.6309	1.4079	1,164.0901	73.4002	0.8836
PuBeCdSingle	-19.6840	2.4039	1,478.2775	125.2398	0.7714
PuBeGdSingle	-11.1191	2.0225	1,157.5541	112.2618	0.6184
CfBareSingle	-9.3092	0.8561	689.8229	29.7001	0.9058
CfCdSingle	-13.0509	1.1859	862.6562	42.9051	0.9201
CfGdSingle	-7.5731	0.5063	653.9373	17.6438	0.9628

Table 23. Calibration Curve linear regressions for all triple pellet alanine conditions.

ID	Intercept Estimate	Intercept SE	Slope Estimate	Slope SE	Adjusted R^2
Cs137Triple	-0.4737	0.1423	28.5961	0.2046	0.9979
PuBeBareTriple	-3.2319	0.9645	441.1900	25.2844	0.9183
PuBeCdTriple	-10.3141	0.8763	621.6220	27.7844	0.9242
PuBeGdTriple	-15.0215	1.4933	875.2511	52.6757	0.8089
CfBareTriple	-4.4915	0.3684	270.1941	6.3305	0.9707
CfCdTriple	-5.7123	0.4673	306.5110	8.3808	0.9745
CfGdTriple	-3.3399	0.3059	256.2385	5.2248	0.9784

PuBe Calibration Curves

Calibration curves for the single and triple pellet conditions were calculated via linear regression and plotted in Figure 28.

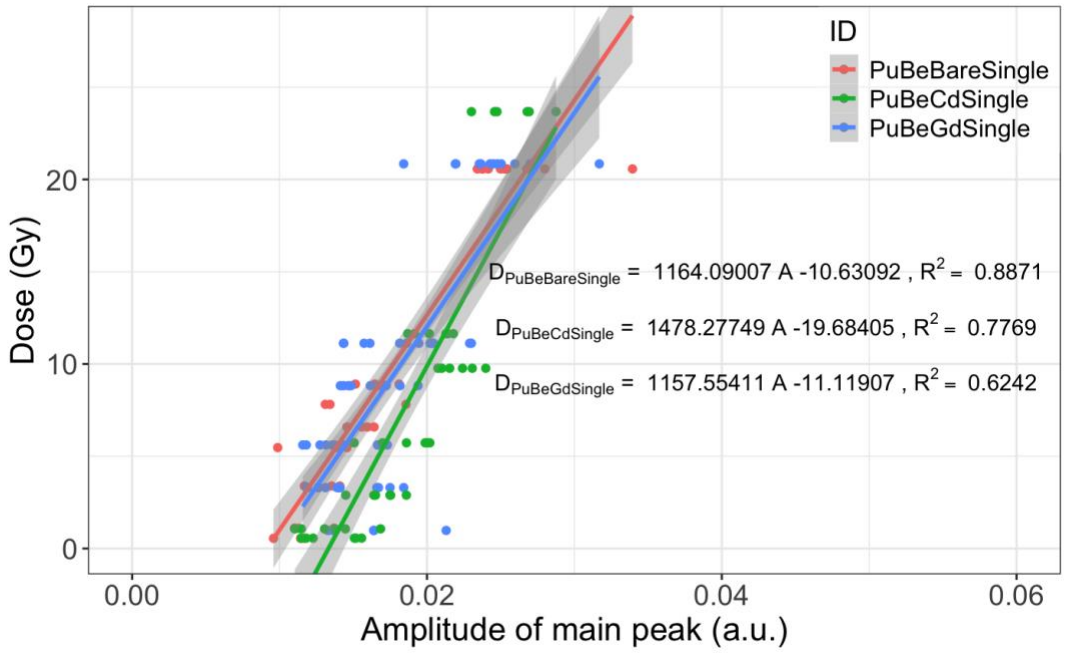

(a)

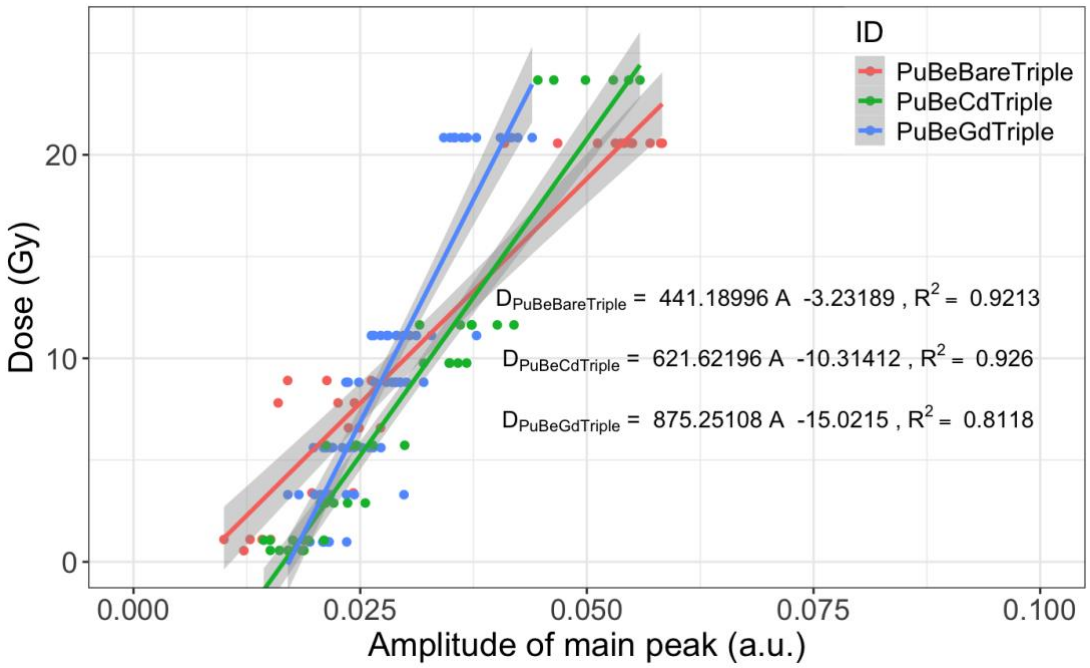

(b)

Figure 28. (a) Linear calibration curves of PuBe Single experimental conditions. 95% C.I. (b) Linear calibration curves of PuBe Triple experimental conditions. 95% C.I.

^{252}Cf Calibration Curves

Calibration curves for the ^{252}Cf single and triple pellet conditions were calculated via linear regression and plotted in Figure 29.

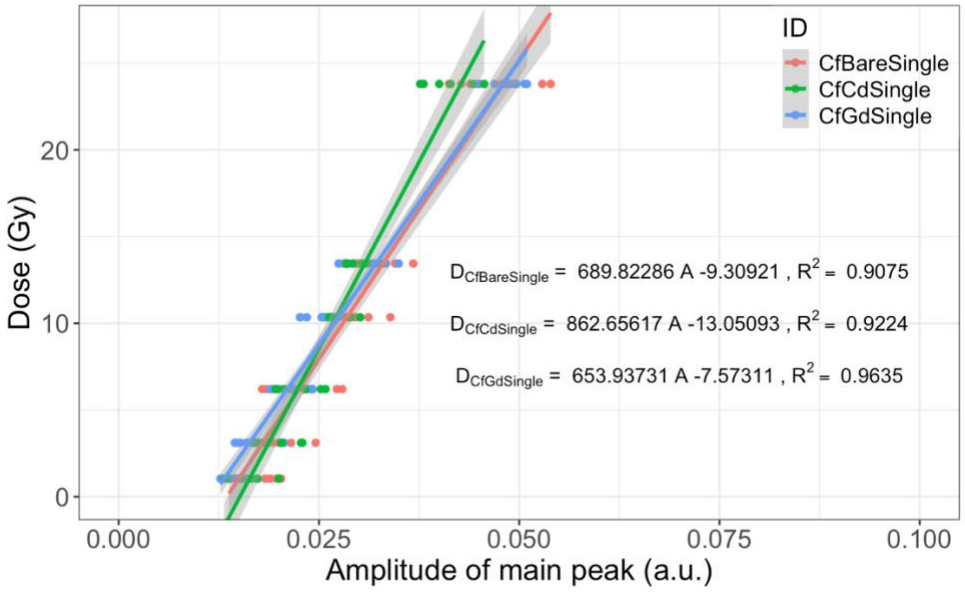

(a)

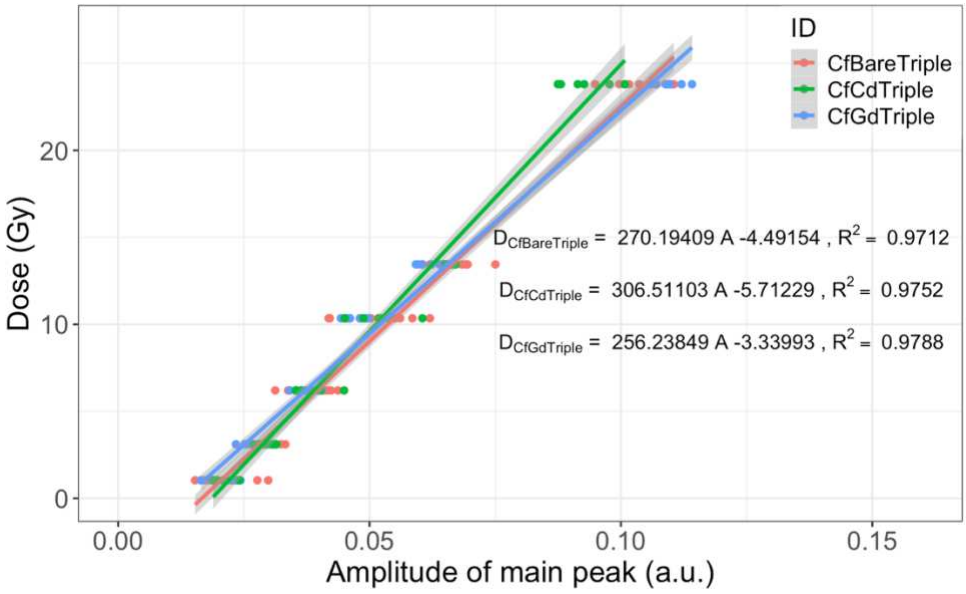

(b)

Figure 29. (a) Linear calibration curves of PuBe Single experimental conditions. 95% C.I. (b) Linear calibration curves of PuBe Triple experimental conditions. 95% C.I.

MCNP Models of Filter Effects

An MCNP model of an alanine pellet and (a) air, (b) a 0.0025 cm thick gadolinium foil, and (c) a 0.0508 cm thick cadmium foil was created to investigate the modeled effects of the foils on gamma and neutron fluence and dose through the alanine pellet (Fig. 30). The source

was a point source 5 cm away from the surface of the alanine pellet, consisting of (i) the measured ^{252}Cf neutron spectrum, (ii) the measured PuBe neutron spectrum, and (iii) monoenergetic photons from 0.2-2 MeV. An F4 (fluence through a cell) and +F6 (collision heating) tally were added to the alanine cell for the fluence and dose values, respectively.

(a) (b) (c)

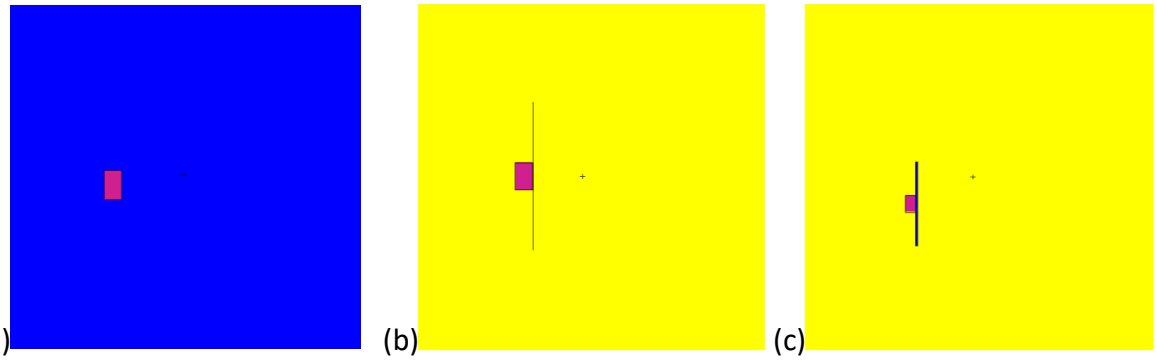

Figure 30. MCNP models of alanine pellets in air with (a) no filter, (b) gadolinium foil, (c) cadmium foil.

At photon energies below approximately 700 keV, a cadmium filter reduces the fluence of photons through alanine (Fig. 31). Below approximately 500 keV, a gadolinium filter reduces the photon fluence through alanine. Thus, the filters may have an impact not only on the alanine's neutron response, but also on the gamma response depending on the incident gamma spectrum.

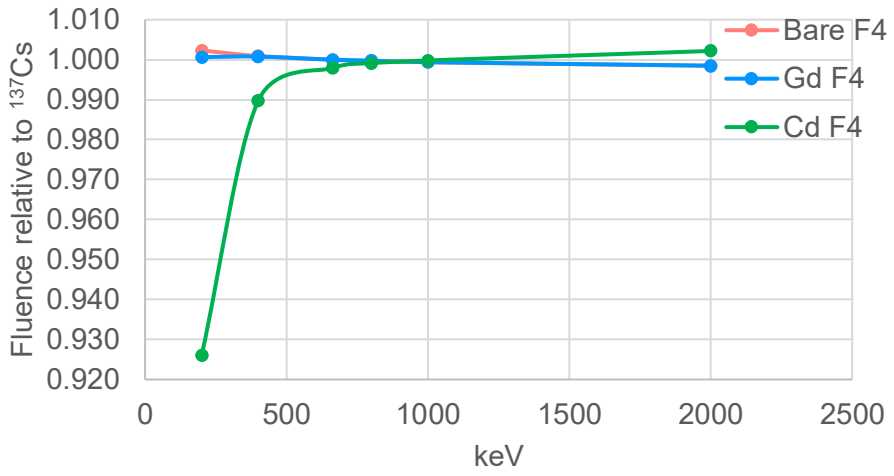

(a)

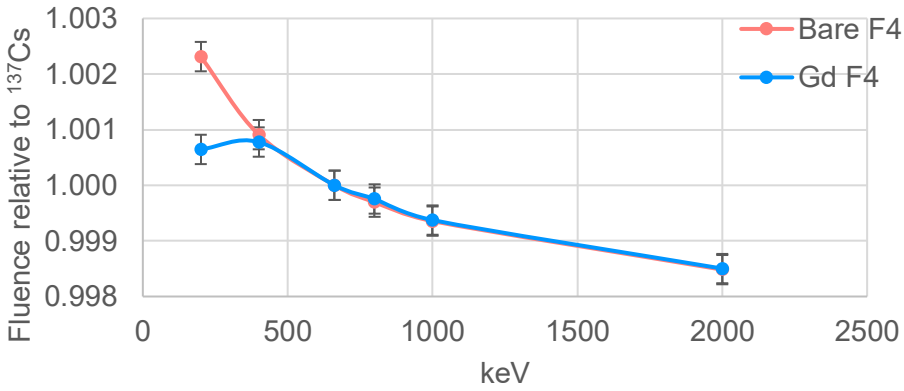

(b)

Figure 31. Gamma fluence (cm^{-2}) through alanine pellet, normalized to ^{137}Cs source (662 keV) (1σ error bars). (b) Cadmium removed.

The cadmium foil reduces the absorbed dose compared to a bare pellet for photons below 662 keV, as could be expected since the fluence through the pellet is reduced by the foil (Fig. 32). However, it is interesting to note that at low photon energies (below 662 keV), the gadolinium foil increases the absorbed dose in an alanine pellet compared to a bare pellet.

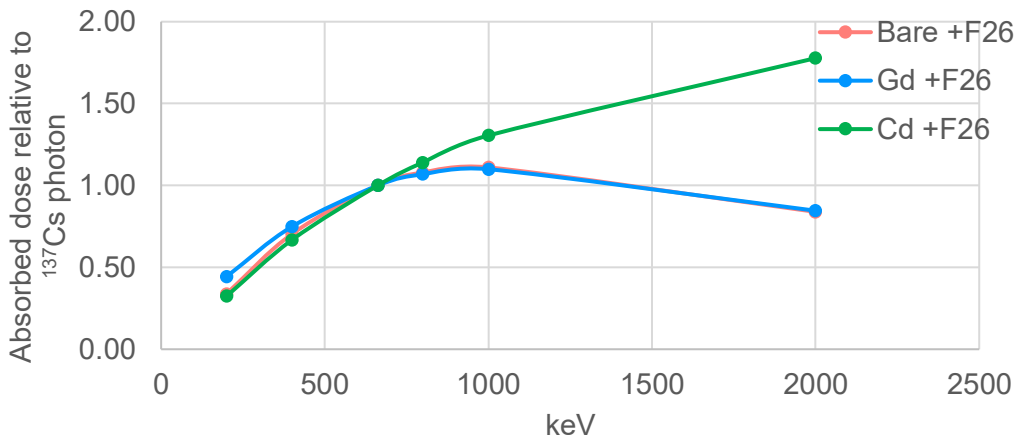

Figure 32. Absorbed dose to alanine pellet due to photons, relative to ^{137}Cs (662 keV) (1σ error bars).

Discussion

No significant qualitative differences were found in the EPR spectra of all the samples after irradiations by ^{137}Cs, PuBe, and ^{252}Cf, with or without neutron filters. Therefore, the relative response of the alanine signal was used to investigate differences between the irradiation sources and filter conditions. The ^{137}Cs source produced a much larger response in bare alanine (dose- response slope: single pellet= 0.0114 ± 0.0002; triple pellet: 0.0349 ± 0.0002) than either the PuBe (dose-response slope: single pellet = 0.0008 ± 0.000; triple pellet = 0.0021 ± 0.0001) or ^{252}Cf (dose-response slope: single pellet = 0.0013 ± 0.0001; triple pellet = 0.0036 ± 0.0001) sources for equal total doses, as well as a more linear fit (Adjusted R^2: ^{137}Cs single: 0.991, ^{137}Cs triple: 0.998; PuBe single: 0.884, PuBe triple: 0.918; ^{252}Cf single: 0.906, ^{252}Cf triple: 0.971). Thus, the method of radiation dose delivery is significant. ^{252}Cf has a higher gamma contribution than PuBe (30% of neutron dose compared to 10% of neutron dose), explaining why it has a higher response to the same total dose. When the gamma contribution is subtracted out, ^{252}Cf still has a higher response to the same neutron dose than PuBe despite the PuBe source having a higher average neutron energy.

Past studies have found fast neutron irradiation sensitivity relative to ^{60}Co gamma sensitivity to be between 0.20 and 0.83, dependent on the energy of the neutrons, the alanine sample type (powder or pellet), and paraffin content (ranging from 10% to 40%) (Katsumura et al. 1986; Trompier et al. 2004). Most of the experiments cited in the literature used reactor spectra and irradiation bursts involving very high dose rates delivered over a short period of time. Thus, this study differs in the low dose rate and long exposure time as compared to the

literature. This, along with the lower neutron sensitivity for both the ^{252}Cf and PuBe source than literature, suggests that there may be another factor influencing the lower neutron sensitivity. Two possibilities are a neutron low-dose dependence or a dose-rate dependence. The neutron doses reported here are much smaller (approximately 0.5-20 Gy) than photon doses reported in literature for development of alanine spectra and dose-response curves (10^3- 10^5 Gy) (Simmons and Bewley 1976; Katsumura et al. 1986). However, there have been experiments of mixed fields in which the total dose to alanine was 2-5 Gy (approximately 1.7 Gy from neutrons) (Trompier et al. 2004). The primary difference was the dose rate: previous experiments used research reactors in which all the dose was delivered in a single burst, not spread over the course of days or weeks. Other experiments do not report the dose rate, but do not include mention of methodology of long-term irradiations (e.g., irradiations over the course of days or weeks). The ^{252}Cf source had a dose rate of 0.090 Gy/h (adjusted lower as source decayed throughout experiment), while the PuBe source had a dose rate of 0.0177 Gy/h. Regulla and Deffner found no dose-rate dependence for gamma irradiations of 10^2 Gy/h - 10^5 Gy/h (Regulla and Deffner 1982), but investigations by NIST found a dose-rate dependence that was also dependent on the absorbed dose (Desrosiers, Puhl, and Cooper 2008; Desrosiers and Puhl 2009). Those investigations found that lower dose-rate irradiations (around 1 Gy/s) produced lower alanine responses to doses above 5 kGy than higher dose rate irradiations (above 2 Gy/s). That work focused on gamma irradiations at dose-rates and absorbed doses (>1 kGy) significantly greater than the present study. The hypothesis was that one or more of the radiation-induced radicals in alanine may be dependent on the dose rate. Therefore, it is hypothesized that the lower alanine response to the neutron+ gamma sources compared to the

^{137}Cs source may in part be explained by the difference in absorbed dose rates. The PuBe source had the lowest neutron sensitivity and the lowest dose rate, perhaps affected by the dose-rate dependence shown. It may also in part explain the difference between published neutron sensitivity data produced by reactor irradiations and this present study. Further investigation into a potential dose rate effect of neutrons at these lower dose rates specifically is warranted.

The impact of the filter foils on alanine response varied by the foil and by the neutron source. The PuBe Cd experiment consistently produced a higher response at lower total doses than the bare alanine in both the single and triple conditions; however, the slope of the bare alanine was larger by 0.0003 ± 0.00005 in the single and 0.0006± 0.00005 amplitude a.u./Gy in the triple condition. This indicates that the absorption of thermal and resonance neutrons did create secondary gamma irradiation that interacted in the alanine pellet and increased the EPR response, but that at some dose the increased response stops, and a reduced response occurs.

At lower doses, the Cf Cd experiment produced a higher response than the bare Cf alanine, but at 5 Gy reach the crossover point and reduced the alanine response. The slope of the bare alanine was larger by 0.0002± 0.00005 and 0.0004± 0.00005 amplitude a.u./ Gy in the single and triple conditions, respectively. The change in response could be due to an effect on the gamma component of the dose response. A ^{252}Cf source has a total gamma spectrum ranging from below 200 keV to above 14 MeV, with 86% of the gamma yield below 1 MeV, 63% below 1 MeV, and 36% below 500 keV (Czakoj et al. 2024). However, below 500 keV, the cadmium foil decreases both the fluence of low energy gammas through an alanine pellet and the absorbed dose to alanine due to gamma radiation (Fig. 31 and Fig. 32). Therefore, when the total dose to alanine is low (and the gamma dose is very low), the cadmium foil may increase

the signal due to neutron irradiation more than it decreases the signal due to the small gamma irradiation. However, as the total dose increases, the gamma dose increases and may become a significant contributor to the bare alanine signal. The cadmium may reduce the gamma dose contribution more than it increases the neutron dose contribution, leading to a cross-over point at which the total response of cadmium-covered alanine is reduced. Since the neutron to gamma ratio was lower for PuBe (gammas contributed 10% of neutron dose) than for ^{252}Cf (gammas contributed 33% of neutron dose), the cross-over region would be higher.

A similar explanation could explain the cross-over behavior of the gadolinium foil in the PuBe. At lower doses of the PuBe source, the gadolinium foil increased the response of alanine as compared to bare alanine for both the single and triple pellet conditions, perhaps due to the reduction in gamma contributions at higher total doses where the gamma contributions more. There was not a statistically significant difference in the ^{252}Cf gadolinium response compared to the bare response, although the observed effect was opposite of the PuBe Gd and both sources' Cd effect. At low gamma energies, gadolinium increases the dose to alanine pellets as compared to a bare pellet. However, at high doses, gadolinium decreased the EPR signal response compared to a bare pellet, perhaps due to an overall decrease in photon fluence through the pellet.

Therefore, this study has found a novel dual effect of filter foils on the EPR response of alanine pellet: the dose-dependent change in response seems due not only to a neutron effect (capture and secondary radiation increasing the response), but also to a gamma effect (changing the fluence of photons through the pellet). Since both effects are energy dependent, the neutron spectrum *and* gamma spectrum would need to be known for each source to

mathematically derive a relationship between the bare and filtered alanine. The gamma spectrum of the PuBe and ^{252}Cf sources have not been measured, and so a mathematical relationship has not been derived for this study.

The triple pellet conditions gave higher linear dose-response relationships (higher Adjusted R^2 values) and provided larger signals in the same measurement time. Given the minimal cost of alanine pellets, it is recommended that future dosimetry methods utilize multiple pellets, with a minimum of two measurements per pellet order, to achieve a more accurate result. If the irradiation conditions change and a calibration curve has not been updated, it is recommended to use the neutron sensitivity value for the specific source and the ^{137}Cs calibration curve to obtain a dose value.

Conclusions

In conclusion, the differential responses of alanine to an expanded collection of radiation fields, spectra, and response filters was shown through the aims of this study: (1) established a dose-response and calibration curve for a ^{137}Cs gamma standard, (2) established a dose-response curve and calibration curve for bare alanine in the mixed neutron+gamma fields, (3) established a dose-response curve and comparison of the bare alanine to filtered alanine in the mixed neutron+gamma fields, calculating neutron sensitivities to each specific experimental condition, and (4) development of a source-specific irradiation procedure to provide dosimetry for future experiments in the mixed fields.

The alanine dosimetry procedure is performed by irradiating pellets in a known field and measuring the relative quantity of induced free radicals using an EPR instrument and the amplitude of the signal. Previous research had investigated gamma sources, neutron sources, and mixed field sources, but the fields in question at CSU were not included. Especially, low dose rate neutron fields had not been investigated. Additionally, the responses of filtered alanine in these fields were unknown prior to this research. Alanine and filtered alanine responses in mixed neutron+gamma fields were investigated to expand on the previous body of work involving alanine-based neutron dosimetry and spectrum analysis.

The development phase of this study involved neutron spectrum and dose characterization in the ^{252}Cf and PuBe mixed neutron+gamma fields of CSU. Neutron spectra from Bonner Sphere unfolding were measured and absorbed dose rates at various points were calculated. The ^{252}Cf source had a higher dose rate and a higher gamma ratio than the PuBe

source at their respective irradiation locations (^{252}Cf absorbed dose rate: 9.04×10^{-2} Gy/h neutron, 3.44×10^{-2} Gy/h gamma; PuBe absorbed dose rate: 1.77×10^{-2} Gy/h neutron, 1.77×10^{-3} Gy/h gamma).

In part two of the development phase, single and triple pellet conditions of bare alanine were irradiated in both sources, as well as the reference ^{137}Cs source. The ^{137}Cs source had a statistically significantly higher dose-response than either neutron source. The neutron sensitivity of the bare alanine in the ^{252}Cf and PuBe sources with reference to the ^{137}Cs source was 0.245 ± 0.212 and 0.056 ± 0.085, respectively. The ^{252}Cf bare alanine neutron sensitivity was within other reported literature values. The PuBe bare alanine neutron sensitivity was lower than reported values, perhaps due to a low dose-rate effect that necessitates the investigation of low dose-rate effects in future research. Calibration curves for each source and pellet number (one and three pellets) were created for use as a dosimetry method for future irradiations.

Part three of this study investigated the effects of filters on alanine response in the neutron fields. Cadmium increased the response of alanine to mixed fields at lower total doses but reduced the response at higher total doses. MCNP models investigating the effect of cadmium on lower energy photons showed that the cadmium filter did not only affect neutrons. It reduced fluence of low energy photons through the alanine pellet, leading to the hypothesis that at lower doses, the increase in alanine response due to neutron interactions in the cadmium increases the overall response. However, when gamma contribution reaches a spectrum-specific proportion of the total dose, the reduction in gamma response due to cadmium overcompensates for the increase in neutron response. The gadolinium had a similar

effect in the PuBe source, but did not have a statistically significant effect in the ^{252}Cf source. Due to the dose dependent effect of the foils, it was not possible to create a linear relationship to isolate the thermal neutron response of the type proposed. Therefore, it is recommended that for future dosimetry needs, the bare calibration curves are used. Other filters such as ^{6}Li could be investigated in future research.

The results of this study offer some caution for future uses of neutron-sensitive materials in alanine dosimetry. In previous studies, EPR signal effects have been attributed solely to neutron interactions. However, this study indicates that photon interactions in the added materials might have a larger effect than expected, dependent on the gamma contribution to the total dose and the gamma spectrum itself.

This study was intended to expand on the methodologies available for neutron dosimetry for dose ranges important in experiment designs (higher doses than routine personnel dosimetry, but lower than industrial uses). While the calibration curves for the available sources were created, shortcomings are present. One limitation of the study was that the mixed source dose-rates used were much lower than dose-rates used in similar work, leading to difficulties in comparing results. Neutron sensitivities were low compared to literature sources, and a potential low dose-rate effect was found. Future projects should investigate the low-dose effect, perhaps in contrast to a higher dose rate source like the deuterium-tritium neutron generator. This source would also provide another neutron sensitivity comparison with the primary contribution of a single neutron energy. Another limitation was that source-specific gamma spectra were not determined. In light of the novel gamma effects of the neutron-sensitive filters, gamma spectra will need to be determined in

future studies to identify the source-specific effect of the filters on both the neutron and gamma measured doses. A last limitation was that the dose unit used throughout the study was personnel absorbed dose. For results to be used in future experiments, dose should be calculated or modified with phantoms or conversion factors specific to the exposure target, for example, a mouse model or a cell model. Additional anticipated areas of research that could expand this project would be to investigate the effect of the filters on different gamma energies; for example, by using a linear accelerator with known photon energies to irradiate an alanine+filter pair. The gamma spectrum from each of the mixed fields could also be measured and modeled in MCNP to determine the source-specific impact of the metal filters on the photon energy incident in the alanine pellets. With a neutron and gamma sensitivity based on the source and filter, spectrum specific information may be obtained.

References

10CFR20. 2002. *10CFR20 Subpart D—Radiation Dose Limits for Individual Members of the Public*. *10CFR20*. Vol. 1301.

ANSI/HPS. 2013. "ANSI/HPS N13.3-2013 (R2019) Dosimetry for Criticality Accidents." ANSI/HPS.

Bartolotta, A., M. Brai, V. Caputo, V. De Caro, L.I. Giannola, R. Rap, and G. Teri. 1999. "ESR Solid State Dosimetry: Behaviour of Various Amino Acids and Blend Preparation Procedures." *Radiation Protection Dosimetry* 84 (1–4): 293–96. https://doi.org/10.1093/oxfordjournals.rpd.a032742.

Boice Jr., J D, R H Clarke, C B Meinhold, Y Sasaki, N Shandala, F A Mettler Jr, W K Sinclair, et al. 2012. "ICRP 103: The 2007 Recommendations of the International Commission on Radiological Protection," October.

Borak, Thomas B., Laurence H. Heilbronn, Nathan Krumland, and Michael M. Weil. 2019. "Design and Dosimetry of a Facility to Study Health Effects Following Exposures to Fission Neutrons at Low Dose Rates for Long Durations." *International Journal of Radiation Biology* 97 (8): 1063–76. https://doi.org/10.1080/09553002.2019.1688884.

Bradshaw, W. W., D. G. Cadena, G. W. Crawford, and H. A. W. Spetzler. 1962. "The Use of Alanine as a Solid Dosimeter." *Radiation Research* 17 (1): 11–21. https://doi.org/10.2307/3571206.

Brown, D.A., M.B Chadwick, R. Capote, and et al. 2018. "ENDF/B-VIII.0: The 8th Major Release of the Nuclear Reaction Data Library with CIELO-Project Cross Sections, New Standards and Thermal Scattering Data." 148: pp. 1-142: Nuclear Data Sheets.

Chadwick, M.B., M. Herman, P. Oblozinsky, and et at. 2011. “ENDF/B-VII.1 Nuclear Data for Science and Technology: Cross Sections, Covariances, Fission Product Yields and Decay Data.” 112(12):2887-2996: Nuclear Data Sheets.

Czakoj, Tomáš, Michal Košťál, Evžen Losa, Stanislav Simakov, Evžen Novák, Martin Schulc, Zdeněk Matěj, Filip Mravec, František Cvachovec, and Roberto Capote. 2024. “Measurement of Total Fission Gamma Spectrum of 252Cf(s.f.).” *The European Physical Journal A* 60 (11): 228. https://doi.org/10.1140/epja/s10050-024-01439-8.

Desrosiers, M. F., J. M. Puhl, and S. L. Cooper. 2008. “An Absorbed-Dose/Dose-Rate Dependence for the Alanine-EPR Dosimetry System and Its Implications in High-Dose Ionizing Radiation Metrology.” *Journal of Research of the National Institute of Standards and Technology* 113 (2): 79. https://doi.org/10.6028/jres.113.007.

Desrosiers, M.F., and J.M. Puhl. 2009. “Absorbed-Dose/Dose-Rate Dependence Studies for the Alanine-EPR Dosimetry System.” *Radiation Physics and Chemistry* 78 (7–8): 461–63. https://doi.org/10.1016/j.radphyschem.2009.03.025.

F. Trompier, C. Huet, R. Medioni, I. Robbes, and B. Asselineau. 2008. “Dosimetry of the Mixed Field Irradiation Facility CALIBAN.” 2008. https://doi.org/10.1016/j.radmeas.2007.11.031.

Gómez-Ros, J. M., R. Bedogni, and C. Domingo. 2023. “Personal Neutron Dosimetry: State-of-the-Art and New Technologies.” *Radiation Measurements* 161 (February):106908. https://doi.org/10.1016/j.radmeas.2023.106908.

Hayes, Robert B., Edwin H. Haskell, Albrecht Wieser, Alexander A. Romanyukha, Byron L. Hardy, and Jeffrey K. Barrus. 2000. “Assessment of an Alanine EPR Dosimetry Technique with

Enhanced Precision and Accuracy." *Nuclear Instruments and Methods in Physics Research Section A: Accelerators, Spectrometers, Detectors and Associated Equipment* 440 (2): 453–61. https://doi.org/10.1016/S0168-9002(99)00957-2.

IAEA, ed. 2001. *Compendium of Neutron Spectra and Detector Responses for Radiation Protection Purposes: Supplement to Technical Reports Series No. 318*. Technical Reports Series / International Atomic Energy Agency 403. Vienna: IAEA.

Katsumura, Y, Y Tabata, T Seguchi, N Morishita, and T Kojima. 1986. "FAST NEUTRON IRRADIATION EFFECTS--Ill. SENSITIVITY OF ALANINE SYSTEMS FOR FAST NEUTRON HAVING AN ENERGY OF ,-~ 1 MeV." *International Journal of Radiation Applications and Instrumentation. Part C. Radiation Physics and Chemistry* 28 (4): 337–41.

Marrale, M., M. Brai, G. Gennaro, A. Triolo, A. Bartolotta, M.C. D'Oca, and G. Rosi. 2007. "Alanine Blends for ESR Measurements of Thermal Neutron Fluence in a Mixed Radiation Field." *Radiation Protection Dosimetry* 126 (1–4): 631–35. https://doi.org/10.1093/rpd/ncm128.

Marrale, M., G. Gennaro, M. Brai, S. Basile, A. Bartolotta, and M. C. D'Oca. 2008. "Exposure of Gd2O3-Alanine and Gd2O3-Ammonium Tartrate ESR Dosimeters to Thermal Neutrons: Experiments and Monte Carlo Simulations." *Radiation Measurements*, Proceedings of the 15th Solid State Dosimetry (SSD15), 43 (2): 471–75. https://doi.org/10.1016/j.radmeas.2007.11.024.

Marrale, M., T. Schmitz, S. Gallo, G. Hampel, A. Longo, S. Panzeca, and L. Tranchina. 2015. "Comparison of EPR Response of Alanine and Gd2O3-Alanine Dosimeters Exposed to TRIGA Mainz Reactor." *Applied Radiation and Isotopes*, The 16th International Congress

on Neutron Capture Therapy (ICNCT-16). Representative person of the Organizing Committee: Dr Hanna Koivunoro (Secretary general of the ICNCT-16), 106 (December):116–20. https://doi.org/10.1016/j.apradiso.2015.08.016.

Marrale, Maurizio, Maria Brai, Gaetano Gennaro, Antonio Bartolotta, and Maria Cristina D'Oca. 2008. "The Effect of Gadolinium on the ESR Response of Alanine and Ammonium Tartrate Exposed to Thermal Neutrons." *Radiation Research* 169 (2): 232–39. https://doi.org/10.1667/RR1138.1.

NRC. 2010. "NRC-Neutron Sources." October 13, 2010. https://www.nrc.gov/docs/ML1122/ML11229A704.pdf.

———. 2011. "NRC Basic Health Physics: Interaction of Neutrons with Matter." February 4, 2011. https://www.nrc.gov/docs/ML1122/ML11229A705.pdf.

Reginatto, Marcel, and Paul Goldhagen. 1999. "MAXED, A Computer Code For Maximum Entropy Deconvolution of Multisphere Neutron Spectrometer Data:" *Health Physics* 77 (5): 579–83. https://doi.org/10.1097/00004032-199911000-00012.

Regulla, D. F., and U. Deffner. 1982. "Dosimetry by ESR Spectroscopy of Alanine." *The International Journal of Applied Radiation and Isotopes* 33 (11): 1101–14. https://doi.org/10.1016/0020-708X(82)90238-1.

Romanyukha, Alexander A. 2021. "Alanine Nuclear Accident Dosimeter. Holder Design and Calibration." Patent Application.

Schraube, H, E Weitzenegger, A Weiser, and D.F. Regulla. 1989. "Fast Neutron Response of Alanine Probes." *International Journal of Radiation Applications and Instrumentation. Part A. Applied Radiation and Isotopes* 40 (10–12): 941–44.

Shuryak, Igor, Helen C. Turner, Jay R. Perrier, Lydia Cunha, Monica Pujol Canadell, Mohammad H. Durrani, Andrew Harken, et al. 2020. “A High Throughput Approach to Reconstruct Partial-Body and Neutron Radiation Exposures on an Individual Basis.” *Scientific Reports* 10 (February):2899. https://doi.org/10.1038/s41598-020-59695-9.

Simmons, J. A., and D. K. Bewley. 1976. “The Relative Effectiveness of Fast Neutrons in Creating Stable Free Radicals.” *Radiation Research* 65 (2): 197–201. https://doi.org/10.2307/3574195.

Stricklin, Daniela L., Jama VanHorne-Sealy, Carmen I. Rios, Lisa A. Scott Carnell, and Lanyn P. Taliaferro. 2021. “Neutron Radiobiology and Dosimetry.” *Radiation Research* 195 (5): 480–96. https://doi.org/10.1667/RADE-20-00213.1.

Stuglik, Zofia. 2007. “Alanine- EPR Dosimetry System. Why We Like It?” *Https://Www.Osti.Gov/Etdeweb/Servlets/Purl/21047760*. December 3.

Trompier, F., P. Fattibene, D. Tikunov, A. Bartolotta, A. Carosi, and M. C. Doca. 2004. “EPR Dosimetry in a Mixed Neutron and Gamma Radiation Field.” *Radiation Protection Dosimetry* 110 (1–4): 437–42. https://doi.org/10.1093/rpd/nch225.

Vega-Carrillo, Héctor René, Eduardo Manzanares-Acuña, Ana María Becerra-Ferreiro, and Aureliano Carrillo-Nuñez. 2002. “Neutron and Gamma-Ray Spectra of 239PuBe and 241AmBe.” *Applied Radiation and Isotopes* 57 (2): 167–70. https://doi.org/10.1016/S0969-8043(02)00083-0.

Waligorski, M.P.R., G. Danialy, K. Sun Loh, and R Katz. 1989. “The Response of the Alanine Detector After Charged-Particle and Neutron Irradiations.” *International Journal of*

Radiation Applications and Instrumentation. Part A. Applied Radiation and Isotopes 40 (10–12): 923–33.

Werner, Christopher J. 2017. “MCNP User’s Manual- Code Version 6.2.” Los Alamos National Security.

Xu, Yanping, Gerhard Randers-Pehrson, Helen C. Turner, Stephen A. Marino, Charles R. Geard, David J. Brenner, and Guy Garty. 2015. “Accelerator-Based Biological Irradiation Facility Simulating Neutron Exposure from an Improvised Nuclear Device.” *Radiation Research* 184 (4): 404–10. https://doi.org/10.1667/RR14036.1.

Appendix A: Bonner Sphere MCNP Model Example

```
Model of the Ludlum 42-5 Bonner Sphere System- 12in detector (BSS_12in)
C
C
#############################################################################
C Model created by Paige Witter at CSU
C
C Version 1.0 created by Paige Witter (CSU) 23/10/2022
C 2/21/2024 materials updated to ENDF/B-V11.1 data tables and thermal scattering,
C         Li-6 crystal changed to RPP, source changed to size of maximum poly
C         sphere
C         NOTE: THIS can be run on MCNP 6.2
C
#############################################################################
C The Bonner Sphere System consists of a 4mmx4mm 6LiI(Eu) crystal, a
C     Plexiglass light pipe, photomultiplier tube, and aluminum casing.
C     6 polyethylene spheres surround the detector to replicate the system.
C
C
#############################################################################
C Cell Cards:
C
#############################################################################
C
C
*****************************************************************************
C Detector body
C
*****************************************************************************
C LiI scintillator crystal
1 1 -4.08 -1          IMP:N=11
C
C Photomultiplier tube
2 2 -1.19 -3 2        IMP:N=9
C
C Air gap around crystal, inside PMT
3 3 -0.001205 -2 1     IMP:N=10
C
C Aluminum casing around PMT
4 4 -2.6989 -4 3       IMP:N=8
C
```

```
C Light pipe
5 2 -1.19 -6 5         IMP:N=1
C
C Aluminum casing around light pipe
6 4 -2.6989 -7 6       IMP:N=1
C
C Air gap inside light pipe
7 3 -0.001205 -5       IMP:N=1
C
C Aluminum casing of body
8 4 -2.6989 -9 8       IMP:N=1
C
C Air inside detector body
9 3 -0.001205 -8       IMP:N=1
C
C Aluminum end plug
10 4 -2.6989 -10       IMP:N=1
C
C
*********************************************************************************
C Bonner spheres: dimension is diameter.
C              Change material to air when not in use
C
*********************************************************************************
C
C 5.1 cm (2 in.) Bonner sphere (CHANGE AIR VS HDPE)
C 100 3 -0.001205 -100 4 7         IMP:N=7  $ AIR
100 5 -0.944 -100 4 7          IMP:N=7  $ HDPE
C
C 7.6 cm (3 in.) Bonner sphere (CHANGE AIR VS HDPE)
C 110 3 -0.001205 -110 100 4 7          IMP:N=6  $ Air
110 5 -0.944 -110 100 4 7            IMP:N=6  $ HDPE
C
C 12.7 cm (5 in.) Bonner sphere (CHANGE AIR VS HDPE)
C 120 3 -0.001205 -120 110 4 7 9         IMP:N=5  $ Air
120 5 -0.944 -120 110 4 7 9            IMP:N=5  $ HDPE
C
C 20.3 cm (8 in.) Bonner sphere (CHANGE AIR VS HDPE)
C 130 3 -0.001205 -130 120 4 7 9         IMP:N=4  $ Air
130 5 -0.944 -130 120 4 7 9            IMP:N=4  $ HDPE
C
C 25.4 cm (10 in.) Bonner sphere (CHANGE AIR VS HDPE)
C 140 3 -0.001205 -140 130 4 7 9         IMP:N=3  $ Air
140 5 -0.944 -140 130 4 7 9         IMP:N=3  $ HDPE
```

```
C
C 30.5 cm (12 in.) Bonner sphere (CHANGE AIR VS HDPE)
C 150 3 -0.001205 -150 140 4 7 9          IMP:N=2  $ Air
150 5 -0.944 -150 140 4 7 9             IMP:N=2  $ HDPE
C
C
C
*********************************************************************
C Geometry outside of detector
C
*********************************************************************
C
C Air surrounding detector
900 3 -0.001205 -900 150 10 9 7 4    IMP:N=1
C
C External universe
901 0 900       IMP:N=0
C

C
#####################################################################
C Surface cards
C
#####################################################################
C
C
*********************************************************************
C    Using macrobodies to define the surfaces:
C    RCC vx vy vz hx hy hz R
C    RPP xmin xmax ymin ymax zmin zmax
C    SO R
C
*********************************************************************
C
C Scintillation crystal at origin:
1 RPP 0 0.4 0 0.4 0 0.4
C
C Photomultiplier tube surrounding crystal
2 RCC -3.8 0 0 4.2 0 0 1.2
3 RCC -3.9 0 0 4.4 0 0 1.43
C
C Aluminum casing around crystal and PMT
4 RCC -4.0 0 0 4.6 0 0 1.6
C
```

```
C Light pipe
5 RCC -9.8 0 0 5.6 0 0 1.8
6 RCC -9.9 0 0 5.8 0 0 1.9
C
C Aluminum casing around light pipe
7 RCC -10 0 0 6 0 0 2
C
C Aluminum casing of body- CHECK LENGTH AND DIAMETER
8 RCC -28 0 0 17 0 0 4.2
9 RCC -29 0 0 19 0 0 5
C
C End plug
10 RCC -31.5 0 0 2.5 0 0 2.5
C
C 5.1 cm (2 in.) Bonner sphere
100 SO 2.55
C
C 7.6 cm (3 in.) Bonner sphere
110 SO 3.8
C
C 12.7 cm (5 in.) Bonner sphere
120 SO 6.35
C
C 20.3 cm (8 in.) Bonner sphere
130 SO 10.15
C
C 25.4 cm (10 in.) Bonner sphere
140 SO 12.7
C
C 30.5 cm (12 in.) Bonner sphere
150 SO 15.25
C
C
C
C General universe
900 RPP -50 50 -50 50 -50 50
C

C
################################################################################
C Data cards
C
################################################################################
C
```

```
C
*********************************************************************
C Mode card: need to track neutrons in the LiI crystal and calculate the number
C          6LiI(n,t)He-4 reactions in the detector sensitive volume.
C        Other options: MODE N P E A if looking at dose tallies. Need to
C          track all particles that could deposit significant energy
C          in the 6LiI(Eu).  Crystal is small therefore both alpha and
C          electrons should be tracked.
C
*********************************************************************
C
MODE N
C
C
*********************************************************************
C Materials: Material composition and density obtained from PNNL Composite
C            Materials Guide, using continuous energy neutron data libraries
C            where available (.80c ENDF/B-V11.1 where available)
C
*********************************************************************
C    LiI Crystal (lithium iodide (High density) enriched in Li-6 (96 %)
M1   3006.80c 0.47999808 3007.80c 0.0199992 53127.80c 0.500002
C
C    Plexiglass (Leucite) PMT
M2   1001.80c -0.080538 6000.80c -0.599848 8016.80c -0.319614
C
C    Air
M3   6000.80c -0.00012 7014.80c -0.75527 8016.80c -0.23178 18000.59c -0.01283
C
C    Aluminium
M4   13027.80c 1.0
C
C    High-density polyethylene (for Bonner spheres)
M5   1001.80c -0.143716 6000.80c -0.856284
MT5  poly
C
C
C
*********************************************************************
C Source definition: Plane parallel mono-energetic source with same dimensions
C                as the sphere. Not valid for diverging sources.
C
*********************************************************************
C
```

```
SDEF X=30 Y=D1 Z=D2 EXT=0 VEC=1 0 0 DIR=-1 PAR=N ERG=2.5e-08
SI1 H -15.25 15.25
SP1 D 0 1
SI2 H -15.25 15.25
SP2 D 0 1
C
C
*********************************************************************
C Tally cards:
C      Note:  SD card replaces the normal divisor (volume for F4) with new
C             values. By overriding the MCNP6-computed cell volume and mass
C             with values of 1, you effectively multiply the unmodified F4
C             by the volume and mass, respectively, yielding the score for
C             the entire cell.
C
*********************************************************************
C
C   LiI Crystal
F4:N 1
FC4 Neutron flux averaged over LiI crystal [neutrons/cm2]
C
F14:N 1
FC14: Neutron absorption 6Li(n,t)He-4 reactions over LiI crystal- ENDF/B-VII.1
E14 1.000E-11 1.103E-11 1.217E-11 1.342E-11 1.480E-11 1.633E-11 1.801E-11
    1.987E-11 2.191E-11 2.417E-11 2.666E-11 2.941E-11 3.244E-11 3.578E-11
     3.947E-11 4.354E-11 4.802E-11 5.297E-11 5.843E-11 6.445E-11 7.109E-11
     7.841E-11 8.649E-11 9.541E-11 1.052E-10 1.161E-10 1.280E-10 1.412E-10
     1.558E-10 1.718E-10 1.895E-10 2.091E-10 2.306E-10 2.544E-10 2.806E-10
     3.095E-10 3.414E-10 3.766E-10 4.154E-10 4.582E-10 5.054E-10 5.574E-10
     6.149E-10 6.782E-10 7.481E-10 8.252E-10 9.102E-10 1.004E-09 1.107E-09
     1.222E-09 1.347E-09 1.486E-09 1.639E-09 1.808E-09 1.995E-09 2.200E-09
     2.427E-09 2.677E-09 2.953E-09 3.257E-09 3.593E-09 3.963E-09 4.371E-09
     4.821E-09 5.318E-09 5.866E-09 6.471E-09 7.137E-09 7.873E-09 8.684E-09
     9.579E-09 1.057E-08 1.165E-08 1.286E-08 1.418E-08 1.564E-08 1.725E-08
     1.903E-08 2.099E-08 2.315E-08 2.524E-08 2.530E-08 2.791E-08 3.078E-08
     3.395E-08 3.745E-08 4.131E-08 4.557E-08 5.026E-08 5.544E-08 6.115E-08
     6.746E-08 7.441E-08 8.207E-08 9.053E-08 9.986E-08 1.101E-07 1.215E-07
     1.340E-07 1.478E-07 1.631E-07 1.799E-07 1.984E-07 2.188E-07 2.414E-07
     2.662E-07 2.937E-07 3.239E-07 3.573E-07 3.941E-07 4.347E-07 4.795E-07
     5.289E-07 5.834E-07 6.436E-07 7.099E-07 7.830E-07 8.637E-07 9.527E-07
     1.051E-06 1.159E-06 1.279E-06 1.410E-06 1.556E-06 1.716E-06 1.893E-06
     2.088E-06 2.303E-06 2.558E-06 2.822E-06 3.112E-06 3.433E-06 3.787E-06
     4.177E-06 4.607E-06 5.082E-06 5.606E-06 6.183E-06 6.868E-06 7.576E-06
     8.356E-06 9.217E-06 1.024E-05 1.129E-05 1.254E-05 1.384E-05 1.516E-05
```

1.660E-05 1.818E-05 2.006E-05 2.213E-05 2.475E-05 2.711E-05 2.969E-05
3.252E-05 3.562E-05 3.875E-05 4.244E-05 4.616E-05 5.021E-05 5.462E-05
5.899E-05 6.461E-05 7.078E-05 7.698E-05 8.373E-05 9.301E-05 1.019E-04
1.124E-04 1.248E-04 1.358E-04 1.477E-04 1.595E-04 1.723E-04 1.900E-04
2.096E-04 2.280E-04 2.463E-04 2.660E-04 2.934E-04 3.236E-04 3.570E-04
3.829E-04 4.164E-04 4.561E-04 5.031E-04 5.589E-04 6.079E-04 6.612E-04
7.344E-04 8.101E-04 8.873E-04 9.788E-04 1.057E-03 1.126E-03 1.251E-03
1.351E-03 1.469E-03 1.587E-03 1.714E-03 1.891E-03 2.100E-03 2.268E-03
2.450E-03 2.644E-03 2.937E-03 3.240E-03 3.524E-03 4.500E-03 5.514E-03
6.523E-03 7.557E-03 8.572E-03 9.522E-03 1.500E-02 2.000E-02 2.416E-02
3.021E-02 3.525E-02 4.500E-02 5.539E-02 6.546E-02 7.553E-02 8.500E-02
9.567E-02 1.007E-01 1.100E-01 1.200E-01 1.300E-01 1.400E-01 1.500E-01
1.600E-01 1.700E-01 1.798E-01 1.900E-01 2.000E-01 2.115E-01 2.200E-01
2.300E-01 2.350E-01 2.385E-01 2.390E-01 2.424E-01 2.450E-01 2.500E-01
2.600E-01 2.700E-01 2.800E-01 3.000E-01 3.100E-01 3.250E-01 3.350E-01
3.500E-01 3.599E-01 3.750E-01 3.850E-01 4.000E-01 4.100E-01 4.250E-01
4.350E-01 4.500E-01 4.632E-01 4.817E-01 4.918E-01 5.000E-01 5.237E-01
5.400E-01 5.700E-01 6.000E-01 6.500E-01 7.000E-01 7.553E-01 8.056E-01
8.560E-01 9.063E-01 9.533E-01 1.007E+00 1.108E+00 1.217E+00 1.337E+00
1.600E+00 1.800E+00 1.913E+00 2.014E+00 2.115E+00 2.216E+00 2.332E+00
2.484E+00 2.618E+00 2.920E+00 3.042E+00 3.122E+00 3.223E+00 3.300E+00
3.400E+00 3.500E+00 3.600E+00 3.700E+00 3.827E+00 3.900E+00 4.129E+00
4.330E+00 4.462E+00 4.600E+00 4.800E+00 4.900E+00 5.000E+00 5.125E+00
5.200E+00 5.300E+00 5.400E+00 5.841E+00 6.000E+00 6.200E+00 6.400E+00
6.500E+00 6.600E+00 6.800E+00 7.000E+00 7.200E+00 7.400E+00 7.500E+00
7.600E+00 7.800E+00 8.000E+00 8.200E+00 8.400E+00 8.550E+00 8.600E+00
9.500E+00 1.005E+01 1.019E+01 1.033E+01 1.048E+01 1.063E+01 1.078E+01
1.093E+01 1.100E+01 1.116E+01 1.131E+01 1.147E+01 1.150E+01 1.166E+01
1.183E+01 1.199E+01 1.216E+01 1.233E+01 1.250E+01 1.268E+01 1.286E+01
1.304E+01 1.322E+01 1.341E+01 1.360E+01 1.379E+01 1.398E+01 1.418E+01
1.438E+01 1.458E+01 1.479E+01 1.499E+01 1.500E+01 1.521E+01 1.543E+01
1.550E+01 1.572E+01 1.594E+01 1.600E+01 1.623E+01 1.645E+01 1.669E+01
1.692E+01 1.716E+01 1.740E+01 1.765E+01 1.790E+01 1.800E+01 1.825E+01
1.850E+01 1.876E+01 1.900E+01 1.927E+01 1.954E+01 1.982E+01 2.000E+01
EM14 47204.4 44945.6 42795 40747.2 38797.4 36940.9 35173.2 33490.2 31887.6
30361.8 28909 27525.6 26208.5 24954.4 23760.3 22623.4 21540.8 20510.1
19528.6 18594.2 17704.4 16857.3 16050.6 15282.6 14551.3 13855 13192
12560.8 11959.7 11387.5 10842.6 10323.7 9829.73 9359.37 8911.52 8485.09
8079.07 7692.48 7324.39 6973.91 6640.2 6322.46 6019.93 5731.87 5457.59
5196.44 4947.79 4711.03 4485.61 4270.97 4066.6 3872.01 3686.73 3510.31
3342.34 3182.41 3030.13 2885.13 2747.08 2615.63 2490.47 2371.29 2257.83
2149.79 2046.92 1948.97 1855.71 1766.91 1682.36 1601.86 1525.21 1452.22
1382.73 1316.57 1253.56 1193.58 1136.46 1082.08 1030.3 980.993 939.531
938.451 893.541 850.78 810.065 771.298 734.385 699.239 665.775 633.911

603.573 574.687 547.183 520.996 496.063 472.325 449.726 428.212 407.734
388.242 369.689 352.025 335.204 319.182 303.92 289.382 275.535 262.343
249.781 237.824 226.445 215.613 205.299 195.477 186.116 177.199 168.715
160.645 152.962 145.642 138.68 132.039 125.707 119.689 113.964 108.518
103.318 98.3851 93.3464 88.8633 84.6135 80.5632 76.72 73.0338 69.5541
66.227 63.0394 60.0277 56.954 54.2302 51.6309 49.1597 46.6408 44.4127
42.1336 40.1203 38.3363 36.6236 34.9911 33.3131 31.7139 29.9848 28.6537
27.3793 26.1561 24.9915 23.9619 22.8922 21.9558 21.0456 20.1814 19.4164
18.5489 17.7235 16.993 16.2952 15.4575 14.7696 14.0614 13.3388 12.7928
12.2642 11.8017 11.3539 10.8099 10.2891 9.86757 9.49343 9.1348 8.695
8.27903 7.88097 7.61153 7.2958 6.96963 6.63492 6.29488 6.03556 5.78765
5.48972 5.22607 4.99303 4.75347 4.57615 4.43154 4.20355 4.04509 3.87785
3.73163 3.59004 3.41827 3.24288 3.12096 3.00289 2.89043 2.74226 2.61121
2.50395 2.21629 2.00373 1.84298 1.71413 1.61165 1.53065 1.228 1.07204
0.982891 0.88991 0.833805 0.756614 0.70534 0.673085 0.654217 0.647423
0.650269 0.655328 0.672939 0.70148 0.74364 0.806937 0.889421 1.00105
1.15482 1.35446 1.62696 1.97053 2.44125 2.80033 3.12933 3.21944 3.2429
3.24394 3.22986 3.20123 3.1007 2.78017 2.39909 2.03676 1.47959 1.28055
1.05541 0.941124 0.81123 0.744143 0.662871 0.618989 0.564827 0.535363
0.497991 0.476524 0.449065 0.429261 0.404342 0.392351 0.383156 0.363069
0.350467 0.33128 0.315747 0.295612 0.28079 0.268322 0.259176 0.251784
0.245896 0.241921 0.238498 0.234307 0.231831 0.230943 0.23053 0.23083
0.230125 0.228031 0.22466 0.220154 0.213664 0.203867 0.19369 0.167798
0.158305 0.152542 0.145903 0.141251 0.136061 0.131751 0.128381 0.126021
0.124465 0.123849 0.120114 0.116063 0.112849 0.108939 0.102091 0.0992824
0.0969944 0.0950435 0.0943366 0.0941044 0.094315 0.0969098 0.0974894
0.0967766 0.09448 0.0927363 0.0901952 0.0844079 0.0764239 0.0696402
0.0639959 0.061487 0.0592409 0.0554447 0.0522046 0.0494083 0.0471377
0.0458071 0.045407 0.0400002 0.0378097 0.0372427 0.0366677 0.0360846
0.0354932 0.0348935 0.0342854 0.034 0.0336896 0.0333749 0.0330557 0.033
0.032351 0.0316929 0.0310255 0.0303486 0.0296623 0.029 0.0286473 0.0282896
0.0279269 0.027559 0.027186 0.0268077 0.0264241 0.026035 0.0256405
0.0252404 0.0248346 0.0244232 0.0240059 0.024 0.0237037 0.0234033 0.0233
0.0229501 0.0225953 0.0225 0.0220485 0.0215907 0.0211264 0.0206556
0.0201781 0.0196939 0.0192028 0.0187048 0.0185 0.0180429 0.0176 0.0171824
0.0168 0.0163175 0.0158282 0.015332 0.015
C
F24:N 1
FC24 Neutron absp: 6Li(n,t)He-4 reactions over LiI crystal- FM Response fxn
SD24 1
FM24 1 1 -2 T
C
C
C

```
C
C
*************************************************************************
C Run condition: In general 10^8 particle histories is sufficient to reduce
C             stochastic uncertainty below 2 %
C
*************************************************************************
C
C       ndp     ndm     mct ndmp dmmp
C prdmp   1.0e+06  2.5e+08  0   4    0
C
NPS 5e7
C
C
#########################################################################
C End of input deck
C
#########################################################################
```

Appendix B: Neutron Energies for Bonner Sphere Modeling and Unfolding

Table B1. Neutron Energies used for Bonner Sphere Modeling and Neutron Spectrum Unfolding

Neutron Energy (MeV)
2.50E-08
5.90E-07
1.20E-06
2.44E-06
4.94E-06
1.00E-05
2.04E-05
4.14E-05
8.41E-05
1.71E-04
3.46E-04
7.03E-04
1.20E-03
1.71E-03
2.44E-03
3.47E-03
4.94E-03
7.04E-03
1.00E-02
1.43E-02
2.04E-02
2.90E-02
4.14E-02
5.90E-02
8.39E-02
1.10E-01
1.31E-01
1.56E-01
1.87E-01
2.23E-01
2.66E-01
3.18E-01
3.79E-01
4.52E-01
5.40E-01
6.44E-01
7.69E-01
9.17E-01

1.10E+00
1.31E+00
1.56E+00
1.87E+00
2.23E+00
2.66E+00
3.18E+00
3.79E+00
4.52E+00
5.40E+00
6.44E+00
7.69E+00
9.17E+00
1.10E+01
1.31E+01
1.56E+01
1.87E+01
2.23E+01

Appendix C: Modeling Neutron Spectra and Dose- MRB 002

A default expected spectrum for the D-T neutron generator at three locations (beamline in MRB 002, operator location in MRB basement, maintenance room on first floor) was modeled in Attila4MC and MCNP using F4 flux tallies and the expected neutron production rate of $1x10^9$ n/s from a generator run at 60 kV. The walls were dry concrete, the generator was aluminum, and the doors were wood (Fig. 33). The Bonner Sphere response functions, the default spectra, and the count rate measurements from the Bonner Spheres were input into the MAXED unfolding code to obtain a neutron fluence at each of the three locations. The additional program Integral Quantities (IQ_FC) was used to obtain the ICRU 57 ambient dose equivalent and integrated fluence rate of the neutron exposure at these locations. Absorbed dose rates were calculated using ANSI/HPS N13.3 Table B.1 fluence-to-absorbed dose conversion factors.

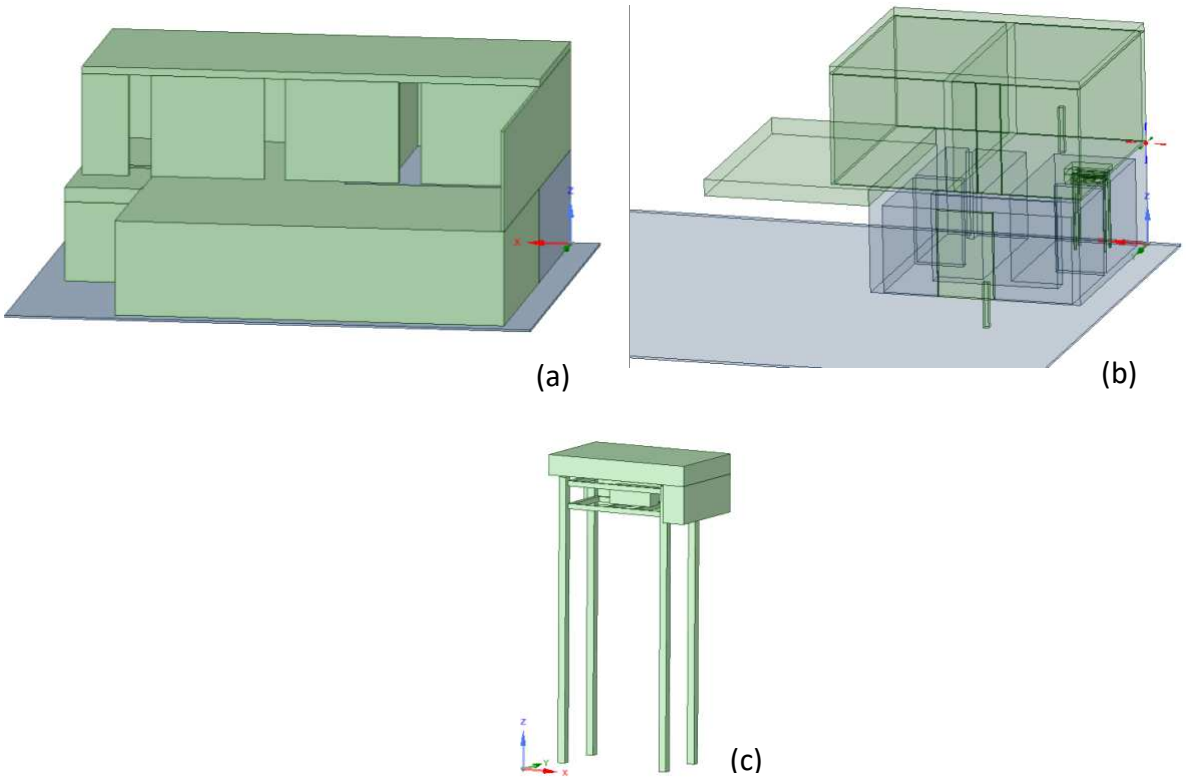

Figure 33. Spaceclaim/ Atilla CAD models of (a) MRB Basement and first floor (solid lines), (b) MRB Room 2 and first floor (shaded lines), and (c) the neutron generator.

MAXED Unfolding-MRB 002 D-T Neutron Generator

A default spectrum for each measurement location was calculated using the MCNP/Atilla4MC geometry and 14.1 MeV source neutrons. This calculation was scaled to the expected neutron output of $1x10^9$ n/s from the source generator. The unfolding code was also run with a normalized neutron spectrum at each location. To obtain the absolute magnitude (i.e., obtain total fluence for an experiment and flux at each location), the resulting unfolded spectrum was scaled with the constant that minimized the algorithm's chi-square value in MAXED.

MCNP Modeling of MRB 002

The fluence at the three locations was modeled for a neutron yield of $1x10^9$ n/s from the DT generator. Enough particles were run to keep the relative error of the models below 0.05.

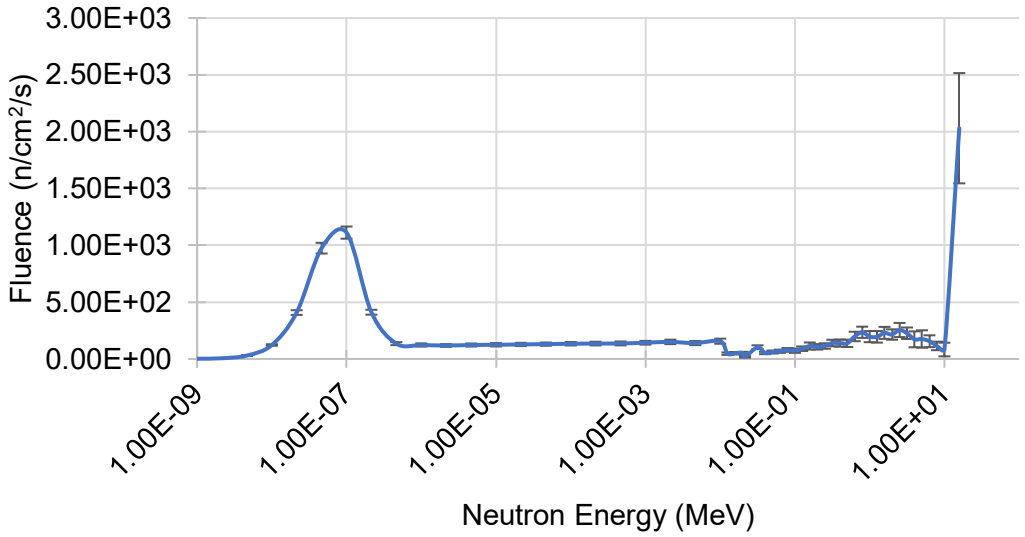

Figure 34. Atilla4MC/MCNP Fluence Calculations at the incubator location with uncertainties at one standard deviation.

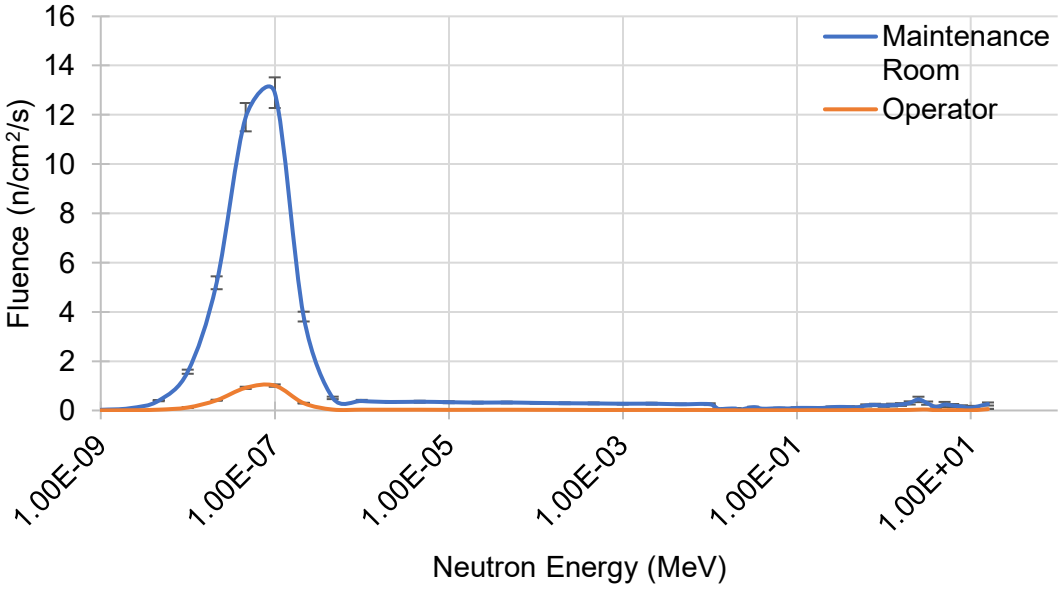

Figure 35. Atilla4MC/MCNP Fluence Calculations at the operator and maintenance room locations with uncertainties at one standard deviation.

BSS Unfolding of MRB 002

Bonner sphere measurements were taken using the Ludlum Model 42-5 BSS system with a Ludlum Model 2200 Ratemeter. The data analyzed were collected using the set of seven detector assemblies, with diameters that ranged from 0 in to 12 in. For the deconvolution, the σ_k were set equal to the square roots of the measured number of counts N_k and ranged from 0.2% to 6% of the N_k. It is estimated that these statistical uncertainties dominated other sources of uncertainty. The main peak of the beamline spectrum is at 14.1 MeV, while scatter throughout the room contributes to lower energy peaks (Fig. 36). ICRU 57 fluence-to-ambient dose equivalent conversion factors were used to calculate the dose rate in the beamline (Table A1).

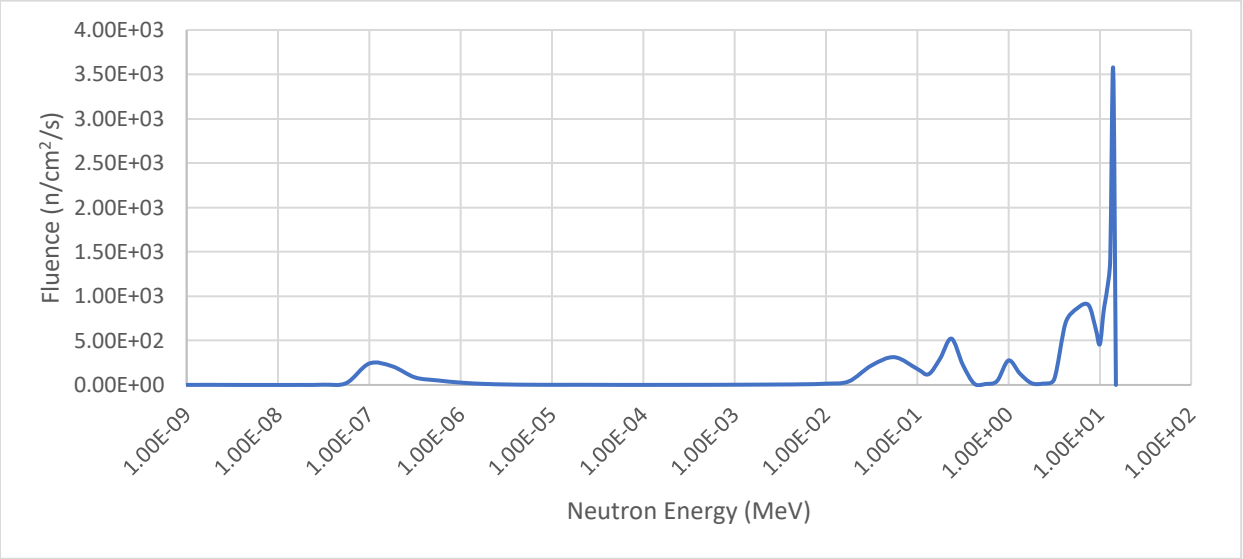

Figure 36. Neutron fluence in the DT generator beamline, unfolded using MAXED.

Table A1. Ambient dose equivalent in DT generator beamline.

BEAMLINE QUANTITY	DOSE RATE (MREM/H)	ABSOLUTE UNCERTAINTY (1Σ)
TOTAL H*(10) DOSE RATE	2.34E+02	1.16E+01
THERMAL NEUTRONS	1.78E+00	1.14E-01
EPITHERMAL NEUTRONS	8.00E+00	6.49E-01
FAST NEUTRONS	1.88E+02	1.10E+01
NEUTRONS >10 MEV	2.86E+01	2.88E+00

The spectra at the operator location and the maintenance room shifted downward, with peaks in the thermal and epithermal energy ranges, along with peaks from 0.1-1 MeV, due to scattering throughout the walls and ceiling (Fig. 37). ICRU 57 fluence-to-ambient dose equivalent conversion factors were used to calculate the dose rate in the two locations (Table A2). Both dose rates (operator location: 0.226 mrem/h, maintenance room: 0.539 mrem/h) fall below the 2 mrem/h dose rate limit for members of the public (10CFR20 2002).

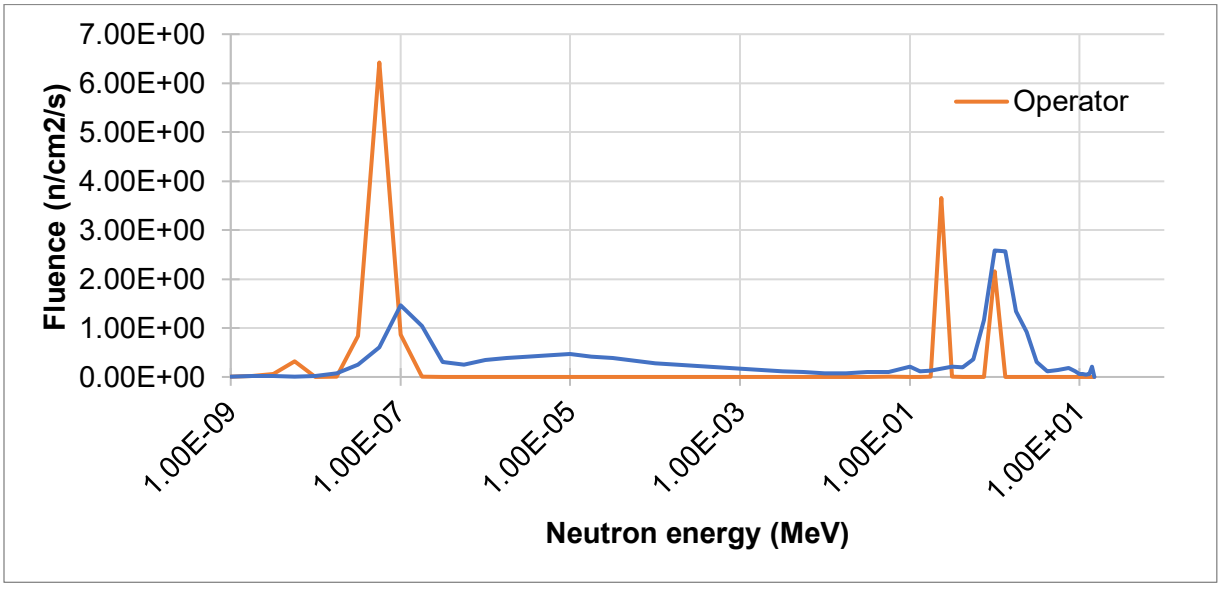

Figure 37. Neutron fluence in DT generator operator location and maintenance room location, unfolded using MAXED.

Table A2. Ambient dose equivalent in DT generator operator location.

Operator	Dose rate (mrem/h)	Absolute uncertainty (1σ)
Total H*(10) dose rate	2.26E-01	1.28E-02
Thermal neutrons	2.94E-02	4.29E-03
Epithermal neutrons	6.35E-05	2.01E-06
Fast neutrons	1.97E-01	2.01E-02
Neutrons >10 MeV	3.09E-27	4.21E-28

Table A3. Ambient dose equivalent in DT generator maintenance room location.

Maintenance Room	Dose rate (mrem/h)	Absolute uncertainty (1σ)
Total H*(10) dose rate	5.39E-01	5.22E-03
Thermal neutrons	1.26E-02	2.47E-04
Epithermal neutrons	1.87E-02	6.90E-04
Fast neutrons	5.03E-01	6.07E-03
Neutrons >10 MeV	1.81E-03	5.69E-04

Due to instrument difficulties, the DT generator was removed from the research plan.

Appendix D: Figure Copywrite Permissions

Figure 2. Radiation weighting factor, w_R, for neutrons versus neutron energy (Boice Jr. et al. 2012).

Permission:

Dear Paige,

Thank you for your response.
On behalf of the ICRP, I am pleased to grant you permission to use Figure 1 of ICRP Publication 103, provided that it is properly cited as originating from ICRP Publication 103 (Ann. ICRP 37 (2-4)).
Best regards,

Keisuke Nakamura, Ph. D.
Assistant Scientific Secretary
International Commission on Radiological Protection
Suite 410, 350 Albert Street, Ottawa, Ontario K1R 1A4, Canada

---

Figure 8. Ludlum Model 42-5 Neutron Ball Cart and Model 2200 Scaler Ratemeter.

Permission:

Hello Paige,
I apologize for overlooking your email on Monday. Congratulations on your work at Colorado State University. You have our permission to use the image of the Ludlum Model 42-5 Neutron Ball Cart in your dissertation, and I've attached a higher-resolution version of the photo for your use. Please include appropriate attribution to Ludlum Measurements, Inc. if your dissertation guidelines require it.

Best of luck with the remainder of your research and writing!

Best regards,

Rebecca Gratehouse
Marketing and Events
rgratehouse@ludlums.com
800-622-0828 ext. 3388
Or dial direct: 325-245-0743